Principles of ion binding to RNA inferred from the analysis of a 1.55 Å resolution bacterial ribosome structure – Part I: Mg^{2+}

Filip Leonarski[1], Anja Henning-Knechtel[2], Serdal Kirmizialtin[2,3], Eric Ennifar[4], Pascal Auffinger[4*]

[1]Swiss Light Source, Paul Scherrer Institut, Villigen PSI, 5232, Switzerland.

[2]Chemistry Program, Science Division, New York University Abu Dhabi, Abu Dhabi, United Arab Emirates.

[3]Department of Chemistry, New York University, USA

[4]Université de Strasbourg, Architecture et Réactivité de l'ARN, Institut de Biologie Moléculaire et Cellulaire du CNRS, 2 Allée Konrad Roentgen, 67084 Strasbourg, France.

* To whom correspondence should be addressed.

Tel: +33 3 88 41 70 00;

Fax: +33 3 88 60 22 18;

Email: p.auffinger@ibmc-cnrs.unistra.fr

ABSTRACT

The importance of Mg^{2+} ions for RNA structure and function can difficultly be overstated. Several attempts were made to establish a comprehensive Mg^{2+} binding site classification. However, such descriptions were hampered by poorly modelled ion binding sites. Recently, ribosome cryo-EM structures with resolutions < 2.0 Å allowed more detailed ion binding site descriptions. However, such a task is challenging. In a recent 1.55 Å *E. coli* ribosome structure (PDBid 8B0X), ion assignment incompleteness/errors were observed that prevent a full understanding of the chelated ion structures. We reinspected this cryo-EM reconstruction by using stereochemical constraints derived from an updated analysis of the Mg^{2+}/K^{+} occurrences in the Cambridge Structural Database (CSD) and established sufficiently straightforward and general binding principles to be applicable to any RNA of sufficient resolution. Through our improved characterization of the RNA ionic structure, we assigned all Mg^{2+} ions bound to 2 up to 4 non-water oxygens leading to a better understanding of the role of Mg^{2+} ions in folding while shedding light on the importance of Mg^{2+}…Mg^{2+}/K^{+} ion pairs in catalytic systems. Based on these data, we defined general Mg^{2+} binding rules allowing to describe unanticipated motifs where up to five adjacent nucleotides wrap around a single ion.

INTRODUCTION

Since the first biochemical investigations on ribosomes, it has become clear that Mg^{2+} along with K^+ and polyamines are essential for the structure and function of these biomolecular systems (1-7). The first ribosome structure that allowed the assignment of mono- and divalent ions was the *Haloarcula marismortui* 50S large subunit (Hm-LSU) by Steitz and co-workers (8). A comprehensive study concerning the identification of Mg^{2+}, Na^+ and K^+ ions was subsequently published by Klein and Steitz (9). Meanwhile, several hundreds of ribosomal cryo-EM/X-ray structures have been deposited to the PDB with resolutions in the 1.55 to > 4.0 Å range (10). The number of assigned Mg^{2+} ions start from zero for the most cautious authors and reaches ≈1260 Mg^{2+} per 70S ribosome (or one Mg^{2+} per three nucleotide) as in the 2.3 Å resolution *Thermus thermophilus* (11) structure (PDBid: 4Y4O) or close to full neutrality as in the 3.1 Å resolution *Thermus thermophilus* (12) structure (PDBid: 4V6F; ≈2970 Mg^{2+}/70S). These numbers are in sharp contrast with the 138 Mg^{2+}, 85 Na^+, 2 K^+, 5 Cd^{2+} cations and 30 Cl^- plus 4 CH_3COO^- anions that were assigned in the latest 2013 refinement (13) of the Hm-LSU structure (PDBid: 4V9F; resolution: 2.4 Å).

According to current knowledge, 100-300 Mg^{2+} ions per ribosome seem a reasonable number depending on ribosome size and cryo-EM/X-ray experimental conditions (2,6). Larger Mg^{2+} numbers result habitually from specific buffer conditions or from an excess of faith in the amount of information contained in experimental data. For RNA and other metal containing biomolecular systems, the latter bias has been documented (14-23) and some tools to identify assignment errors have been developed (24-26) but none specific to nucleic acids besides the MgRNA attempt (27) that has been critically evaluated (14,15).

Thus, it is essential to advance our understanding of the binding stereochemistry of Mg^{2+} and K^+ ions to rRNA to correctly assign these ions to the peaks derived from experimental cryo-EM/X-ray density maps and to get more insights into their biological functions. For that, we re-examined the recent *Escherichia coli* 70S ribosomal cryo-EM structure (10) that was solved at a stunning 1.55 Å resolution (PDBid: 8B0X) and that comprise 1 Zn^{2+}, 361 Mg^{2+}, 168 K^+ and 11461 water molecules. A rapid examination of 8B0X made us realize that some Mg^{2+} ions have incomplete octahedral coordination shells and that K^+ displaying coordination distances close to 2.8 Å were wrongly assigned as Mg^{2+} ions (**Figure 1**). Such incorrect/imprecise assignments are a hurdle to database surveys (19,27) and to the development of artificial intelligence (AI) tools that might produce improper results when fed with poor quality data (28-32). These observations prompt towards more thorough examinations of already published models of the ribosome solvation shell to progress in automatic assignment techniques.

The aim of the present study is to apply state-of-the-art stereochemical knowledge to define criteria to validate the ionic structure of small RNAs up to large ribosome structures by correcting inaccurate assignments such as those that have been addressed in earlier reports (14-16,18). This will help to build the foundation of a complete "prior knowledge" Mg^{2+}/K^+ ion binding site classification. For that, we inspected one by one all 8B0X ion positions and report new binding sites in regions where the water structure was only partially explored.

We first present an updated classification of Mg^{2+} binding sites based on MgRNA (14,15,27). We illustrate each of the uncovered ion binding site classes and discuss the formation of novel motifs

including, among others, Mg^{2+} bound O2' atoms. We also describe the occurrence of Mg^{2+}…Mg^{2+} and Mg^{2+}…K^{+} ion pairs that are recurrently observed in catalytic systems. Based on these data, we defined a set of simple stereochemical rules to place Mg^{2+} ions at key binding locations. Among those locations, we stress the importance of Mg^{2+} binding clamps and demonstrate that by scanning the OP…OP distances below 3.4 Å, we are able to detect close to 100% of Mg^{2+} bidentate clamps that we consider to be the most important Mg^{2+} binding motifs involved in ribosome folding events occurring during biogenesis.

Besides rules allowing to place Mg^{2+} chelated to two or more non-water O/N atoms, we present also rules to characterize the binding of $Mg(H_2O)_6^{2+}$ ions that are based on a correspondence between the local rRNA hydration structure and that of the Mg^{2+} hydration shell, therefore, reminding rational drug design strategies. For Mg^{2+} ions bound to a single non-water O/N atom, mixed rules based on both, idiosyncratic properties of the ions when coordinated to O/N atoms and, as for $Mg(H_2O)_6^{2+}$ ions, on a correspondence between the rRNA and the Mg^{2+} hydration shell can be used. In that respect, we underline the importance of thoroughly refining the solvation shell of these systems even when the 1.5 Å resolution limit was reached. Such a process is central to a better understanding of the ion binding process.

Finally, we address the role of Mg^{2+} in establishing bridges between ribosomal domains and at the SSU/LSU and r-protein interfaces. These findings may be applied to the exploration of the solvation shell of a large number of nucleic acid systems. They lead to a better understanding of the ion binding rules that, in turn, may help develop better designs for the structures used to start molecular dynamics (MD) simulations and serve as a sound reference point to investigate RNA solvation shells of bacterial and other ribosomal structures (28,33-39). However, even by examining high-resolution structures, the $Mg(H_2O)_6^{2+}$ and K^{+} ions of the diffuse type that take the most significant part in the charge neutralization process escape to any direct observation and will have to be characterized by using MD simulations as already done for smaller fragments such as RNA helices (39-46). In that respect, we discuss the high ionic conditions used to derive the 8B0X structure and compare them to the *in vivo* ionic conditions that are optimal for ribosomal activity.

Of course, this study relies on the exploration of a single bacterial ribosomal structure. Yet, we stress that 8B0X is probably the best candidate to explore the ionic shell of ribosomal systems, including mitochondrial ones (47), given that it has currently the best resolution. Moreover, given conservation of the ribosomes core sequence and structure we believe that a significant proportion of the chelated ions present in *E. coli* ribosomes are present in other archaea, bacterial and eukaryote ribosomes (9,48,49).

As we realized that the Mg^{2+} binding site description would be quite extensive, we refrained to discuss in this report the idiosyncratic binding features of K^{+} ions. The latter will be addressed in a companion paper that will complete recent investigations on this topic (14,50).

METHODS

8B0X cryo-EM buffers

To best evaluate solvent density maps, a good understanding of the experimental buffer compositions is essential. The final buffer used to stabilize the "strain B" 8B0X ribosome (10) contained 25 mM $Mg(OAc)_2$, 100 mM K(OAc), 50 mM HEPES, and 1 mM DTT for a pH of 7.4. Thus, besides HEPES and DTT, only Mg^{2+} and K^+ cations along with acetate anions and water molecules are theoretically contributing to the cryo-EM solvent density map. Notes related to details of this and other high-resolution *E. coli* structures are provided in the **SI**.

Updated CSD histograms for Mg and K

Distance and angle histograms related to the Mg^{2+} and K^+ ions were derived from the Cambridge Structural Database (CSD version 5.43, update November 2022; see **Figure 2/3**) (51,52). These histograms are updated versions of those presented earlier (14,15,53). Only good resolution structures where considered (R_factor ≤ 0.05 %) while disordered, error containing, polymeric and powder structures were discarded. All O/N atom types were considered with the exception of protonated nitrogens that do not contact cations. Charge constraints were not applied since the attribution of charges is sometimes random in the CSD (54). We considered only hexacoordinated Mg ions since it is their prefered coordination mode in a nucleic acid environment. Potassium (K) coordination can range from six to nine. Hence, no restrictions on the number of coordinated atoms were applied for this ion.

Mg coordination parameters

Average coordination distances for hexacoordinated Mg derived from the CSD histograms are *d*(Mg…O) ≈2.07±0.04 Å and *d*(Mg…N) ≈2.19±0.08 Å (**Figure 2**). A 2.3–3.6 Å exclusion zone can be inferred for Mg indicating that no O/N atoms should be present in this distance range. Slightly longer *d*(Mg…N) coordination distances are observed in the CSD histograms. The origin of these offsets remains undocumented although it might in part be related to the bulky imidazole rings that are the only significant nitrogen containing ligands in biomolecular systems (55). For Mg, the coordination angles for ligands in *cis*- and *trans*- are θ(O…Mg…O) ≈90±3° and θ(O…Mg…O) ≈177±4°. The resulting average distances between O/N ligands in *cis*- and *trans*- are *d*(O…O) ≈2.93±0.09 Å and ≈4.13±0.07 Å (**Figure 3**). Coordination parameters for K are discussed in the **SI**.

Ion binding site nomenclature

The present ion binding site terminology, that has been extended to comprise amino acid atoms, is derived from the MgRNA nomenclature (14,15,27). O_{ph} corresponds to OP1/OP2 phosphate anionic oxygens, O_r to O2'/O4'/O3'/O5' ribose and phosphate bridging oxygens, O_b to nucleobase O2/O4/O6 oxygens and N_b to non-protonated nucleobase N1/N3/N7 nitrogens. Ion binding sites are named through a combination of these categories. For Mg^{2+} and other hexacoordinated ions, this nomenclature uses the *cis-/trans-* and *fac-/mer-* terminology (27). Thus, $2O_{ph}.4O_w$ stands for a hexacoordinated ion bound to two O_{ph} atoms and four waters. Accordingly, the sites with two O_{ph} atoms in *cis*- or *trans*- and four water molecules are named *cis*-$2O_{ph}.4O_w$ and *trans*-$2O_{ph}.4O_w$. When three non-water ligands such as O_{ph} are attached to the ion, these isoforms become *fac*-$3O_{ph}.3O_w$ (*facial*) when the three O_{ph} pairs are in *cis*- and *mer*-$3O_{ph}.3O_w$ (*meridian*) when at least one O_{ph} pair is in *trans*- (27). When four non-

water atoms are bound to the ion, the *cis-/trans-* terminology is used by monitoring the respective position of the two bound water molecules instead of that of the coordinated O_{ph} atoms. To distinguish them from the cis-/trans-$2O_{ph}.4O_w$ types, the *Cis-/Trans-* prefix starting with a capital letter is used. Finally, this *cis-/trans-/fac-/mer-/Cis-/Trans-* nomenclature can be extended to atoms of the O_b/N_b types. For proteins, we used O_{back} for amino acid backbone oxygens, O_{coo} for Asp/Glu carboxyl oxygens, O_{cno} for Asn/Gln carbonyl oxygens, OH_{prot} for Ser/Thr/Tyr hydroxyl oxygens and N_{His} for non-protonated ND1/NE2 histidine nitrogens.

Phenix refinements

Since very few structures deposited to the PDB are flawless, we used the outputs of the "*IonDiagnosis*" tool we developed earlier (16) to identify stereochemical issues and ion misassignments in the 8B0X structure (see **SI** for the "*IonDiagnosis*" output for the 8B0X structure) and to correct them through the addition of 2.07 Å coordination distance restraints for Mg^{2+}. The resulting Mg^{2+} coordination shell allowed a more in-depth ion binding site survey that would have been more challenging to collect with Mg^{2+} ions presenting following flaws: *(i)* coordination distances exceeding the 2.3 Å limit, *(ii)* incomplete coordination shells or *(iii)* unassigned ions as observed in the original 8B0X structure (**Figure 1**). After defining the appropriate distance restraints, the 8B0X structure was refined in Phenix (56). We refrained to use angle restraints that would have led in our opinion to an inappropriate level of idealization (see next paragraph). In addition, we made several other changes like removing water molecules with short contact distances and adding water molecules to unassigned density patterns. This resulted in an amended 8B0X model with a more complete and stereochemically correct solvation shell. The amended 8B0X coordinate file is available from the authors upon request.

Coherency criteria used to check the assigned Mg^{2+} ion binding sites

We used several criteria to estimate the coherency of the identified ion binding sites. For Mg^{2+}, we first checked whether six coordination distances close to 2.07 Å were present. Then, the octahedral character of the ion coordination shell was checked by calculating the angular deviations of the bound atoms. For that purpose, the hexacoordinated Mg^{2+} ions were classified into one of the three categories: "correct", "slightly distorted" and "highly distorted". These categories are determined based on the deviation of the cumulated (ligand…Mg^{2+}…ligand) angle value from a regular coordination octahedron: less than 5° for "correct", in the 5-10° range for "slightly distorted" and more than 10° for "highly distorted". The ions in the "highly distorted" category display stereochemistry's that are significantly affected by local disorder, partial occupancy or any other factor that might blur their coordination pattern. As such we refrained to include these ions in the statistics of our survey unless otherwise specified. However, we included them in our final 8B0X model.

A second coherency criteria was defined as follows: if the density peak of a given ion is below an arbitrary value of 4.0 r.m.s.d. as defined by the Coot visualization program (57), this ion was not used in our Mg^{2+} binding pattern evaluation. Further, if some coordinating atoms are found in the 2.3–3.4 Å exclusion range region, we tried to correct the stereochemistry of the binding site. If we were unable to find any rational for these "exclusion zone" contacts, we rejected these ions from our survey. The discarded sites might have been at least partially correctly modelled but the experimental density maps were not sufficiently precise to interpret the observed patterns. The coherency criteria used to check

the K^+ assignments are given in the **SI** as well as an EXCEL file describing all uncovered ion binding sites of the amended 8B0X structure.

RESULTS

Amendments to the solvent structure of the 8B0X ribosome

Mg^{2+} ions are hexacoordinated with d(Mg^{2+}...O/N) ≈2.07/2.19 Å. Based on previous knowledge and on our CSD survey (**Figure 2**), we assume that the preferred Mg^{2+} coordination number is six in most biochemical environments with a strict coordination distance of 2.07±0.04 Å and a slightly longer 2.19±0.08 Å coordination distance to purine N7 and non-protonated histidine ND1/NE2 nitrogens. Despite the exceptional 1.55 Å resolution of 8B0X, a rapid inspection of the structure deposited to the PDB and of the corresponding "*IonDiagnosis"* file (see **SI**) reveals that only 96 of the 361 assigned Mg^{2+} ions are hexacoordinated with coordination distances in the 1.9–2.3 Å range. Moreover, 232 of the latter have an incomplete coordination shell or display at least one coordination distance exceeding 2.3 Å (**Figure 1**).

To establish a comprehensive classification of Mg^{2+} ribosomal binding sites, we completed whenever possible their coordination shell and added 104 hexacoordinated Mg^{2+} ions to non-assigned density spots. We also added during subsequent Phenix refinements *d*(Mg^{2+}…O/N) ≈2.07/2.19 Å coordination distance restraints, thereby assuming a rigid Mg^{2+} coordination octahedron. However, we did not use angle restraints. Through that process a much clearer Mg^{2+} coordination picture emerged. However, other "fixes" where necessary. For instance, 28 assigned Mg^{2+} ions with coordination distances in better agreement with those of K^+ were reassigned (**Figure 1**). Similarly, two K^+ ions were reassigned as Mg^{2+}. Yet, the coordination of a sub-category of Mg^{2+} ions appeared significantly distorted implying that the local experimental densities are too blurred to correctly model their coordination shell (see **Methods**). These ions were not used to define the Mg^{2+} binding site categories described below but were still associated with possible Mg^{2+} coordination events and included in our amended 8B0X model. For some Mg^{2+}, it was impossible to define a hexacoordinated pattern. This resulted in the deletion of ≈40 of them or their mutation to water. It was also necessary to slightly readjust the upper limit of the Mg^{2+} exclusion zone from 3.6 to 3.4 Å (see **SI**) to take into account specificities related to ions coordinated by more than two non-water oxygen atoms.

Finally, all densities close to rRNA/r-protein atoms were inspected to recover ≈110 Mg^{2+} ions that were either assigned as water molecules K^+ ions or not assigned at all (**Figure 1**). Although it is documented that anions can bind to nucleic acids (58,59), we were unable at this stage to assign acetate anions or HEPES/DTT molecules (see **SI**). To summarize, the initial model contains 361 Mg^{2+}, 168 K^+ and 11,461 water molecules whereas the final model contains a total of 403 Mg^{2+}, 231 K^+ and 21,397 water molecules with 299 Mg^{2+} positions in common.

Mg^{2+} binding motif description. The ion identification process described above allowed a clear-cut classification of Mg^{2+} ion binding sites in 8B0X in terms of type and frequency. Of course, given that the resolution of cryo-EM structures weakens with the distance to the centre of the ribosomal particle, the atomic models associated with some regions of the structure are less precise. This is the case for a large part of the SSU. However, we consider that the assigned 403 Mg^{2+} ions (290 well-defined) correspond to a significant part of the chelated divalent ions necessary to the stabilization of the

bacterial ribosome. Next, we describe the classification of these sites that are schematized in **Figure 4** along with their occurrence as characterized in the amended 8B0X structure.

• $6O_w$ coordination (79 well-defined occurrences among 115): Hexahydrated outer-shell coordination modes involve only 2nd shell hydrogen-bonds. In principle, a $Mg[H_2O]_6^{2+}$ ion can establish up to 12 hydrogen-bonds. Yet, such a high number has not been observed in 8B0X where the number of 2nd shell water-mediated contacts is in the 1–8 range (**Figure 5A**) with an average number close to ≈4 if we consider the 79 well-defined ions with density peak values > 4.0 and with an octahedral deviation value < 10°. Given their large diversity, it is difficult to individually describe all $6O_w$ binding patterns. However, a few of their characteristics can be mentioned. For instance, the best hydrogen bond acceptors are the deep groove O6/N7 guanine atoms and the OP1/OP2 phosphate group oxygens with a slight preference for the OP2 atoms. Among the 79 well-defined ions, 45 of them contact both O6/N7 atoms and 9 contact only one of these atoms. Further, 16 ions contact OP1/OP2/O2' atoms while 63 contact a combination of nucleobase and phosphate group atoms (**Figure 5A**).

When $Mg[H_2O]_6^{2+}$ establishes water-mediated contacts to a guanine Hoogsteen edge, the two water molecules bound to the O6/N7 atoms can replace two Mg^{2+} first shell water molecules in *cis*-. This process takes advantage of the comparable ≈2.8–3.0 Å distance separating the two pairs of water molecules (**Figures 3/5B**). Although a recurrent $6O_w$ binding pattern to the guanine Hoogsteen edge emerges, this binding pattern is not unique as numerous structural shifts associated with sequence variations can perturb it. For instance, when an ion binds to the deep groove of a Watson-Crick pair, it tends also to establish water-mediated contacts to the nearby OP2 atoms. This suggests that the guanines with an accessible Hoogsteen edge are an excellent anchor point for accommodating $Mg[H_2O]_6^{2+}$ ions (9,27).

Besides the major groove oriented OP2 atoms, the binding to OP1 atoms is more characteristic of shallow groove contacts associated with diverse loops and interhelical motifs. **Figure 5A** shows a Mg^{2+} "bridging water" that attaches to two O_{ph} atoms from consecutive nucleotides. Such recurrent binding motifs also illustrated in other figures of this paper will be explored elsewhere. Due to reduced accessibility, the O2'/O3'/O4'/O5' atoms are rarely involved in 2nd shell hydrogen-bonds as are the purine N3 and the pyrimidine O2 atoms. To summarize, there is a preference for the binding of $6O_w$ ions to guanine-rich major grooves although, depending on the structural context, any combination of OP1/OP2/O_b/N_b atoms can be part of the 2nd coordination shell of $Mg[H_2O]_6^{2+}$ ions.

• $O_{ph}.5O_w$ coordination (105 well-defined occurrences among 147): This coordination mode is the most frequent and involves OP1/OP2 atoms with a slight preference for the OP2 atoms (46 versus 59). Again, the coordinated water molecules may or may not establish water-mediated contacts with rRNA or r-protein atoms. In a rather exceptional environment and in addition to one inner-shell O_{ph} bond, up to ten water-mediated contacts were observed for a single $O_{ph}.5O_w$ ion. This is the most highly connected Mg^{2+} observed in 8B0X (**Figure 6A**). This stunning motif involves five consecutive nucleotides that wrap around the ion.

When bound to a single phosphate group, the (P-OP…Mg^{2+}) angle is ≈148±10° (**Figure 6B**). Importantly, the bound Mg^{2+} is mainly located in the OP1–P–OP2 plane with an average deviation of ≈0.7±0.3 Å (**Figure 6B**). 97 of the $O_{ph}.5O_w$ ions (**Figure S1**) are in *syn*- with respect of the phosphate

groups and only 8 are in *anti*- if we consider a nomenclature developed for carboxylate groups (60). We did not observe the "bidentate" type of coordination (61,62) that implies that Mg^{2+} interacts with both oxygen atoms of a carboxylate or phosphate group (**Figure S1**). With 15 binding occurrences, the guanine Hoogsteen edge is, as for $6O_w$, an excellent anchor-point for water-mediated contacts involving $O_{ph}.5O_w$ ions (**Figure 6A**). As discussed below, these rather strict constraints are useful to define rules for an automatic or semi-automatic ion placement.

• $O_b.5O_w$ coordination (10 well-defined occurrences among 16): These patterns are rare and involve the (G)O6, (U)O4, (PSU)O2 and (C)O2 atoms. When compared to the $6O_w$ and $O_{ph}.5O_w$ coordination types, binding to O_b atoms is only possible in rare structural contexts the characteristics of which could not be establish yet (**Figure 6C**). An example of $O_b.5O_w$ coordination was reported in a P4-P6 group I intron structure (14). In most instances, the Mg^{2+} ion turns to the Hoogsteen edge but can also be oriented towards the nucleobase Watson-Crick edge. The C=O…Mg^{2+} angle is ≈144° and Mg^{2+} is strictly in the nucleobase plane (14,46).

• $N_b.5O_w$ coordination (7 well-defined occurrences among 10): These patterns are less frequent and involve mostly the (G)N7 atoms. Direct Mg^{2+} coordination to N1/N3 atoms is not observed and coordination to the (A)N7 atom, although possible, is only observed in more complex motifs (see below). Indeed, the guanine Hoogsteen edge is more electronegative than the adenine Hoogsteen edge (**Figure 6D**). The density patterns in the vicinity of the N7 atoms are often blurred and difficult to interpret as discussed in Ref. (63). Binding events to N7 atoms were considered in several instances to be important for catalytic mechanisms but it has been stressed that they are quite rare (15,64).

• *cis*-$2O_{ph}.4O_w$ coordination and variations (35 well-defined occurrences among 47): *cis*-$2O_{ph}.4O_w$ coordination modes can be split into two main categories involving adjacent (17 occurrences) and sequence distant nucleotides (18 occurrences). The first category (**Figure 7A**) was defined as bidentate Mg^{2+} clamps (27,48,64,65). These motifs were also defined as 10-membered ring systems (Mg^{2+}–OP–P–O5'–C5'–C4'–C3'–O3–P–OP) and involve any combination of OP1/OP2 atoms whereas the most common combination involves the deep groove OP2/OP2 atoms. Other patterns comprise O_{ph} atoms from distant residues. The later patterns sometimes bridge different rRNA domains through inner-shell contacts (**Figure 7B**). In a few instances, a clamp involving a Mg^{2+} bridging an $O_{ph}(n)$ and an $O_{ph}(n+2)$ atom occur. These were considered as new motifs and called 16-membered ring systems but are merely a variation of the 10-membered ring system (29).

Importantly, there is a strict correspondence between the distance separating two Mg^{2+} first shell water molecules in *cis*- and the ≈2.9 Å distance separating two coordinated O_{ph} atoms (**Figure 3**). Therefore, it can be stated that Mg^{2+} ions stabilize short O_{ph} contacts by imposing a $d(O_{ph}…O_{ph})$ distance that corresponds to the distance separating two of their 1st shell water molecules. As detailed below, all short $d(O_{ph}…O_{ph})$ ≈2.9 Å observed in 8B0X are stabilized directly or indirectly by a Mg^{2+} ion.

Variations of this motif involve the replacement of one or two O_{ph} atom by O_b/N_b atoms. Eight well-defined occurrences are of the *cis*-$O_{ph}.O_b.4O_w$ type, two are of the *cis*-$O_{ph}.N_b.4O_w$ type and two of the *cis*-$O_{ph}.4O_w.N_{His}$ type while one poorly defined occurrence is of the *cis*-$2O_b.4O_w$ type and involves (C)O2 and (G)O6 atoms. The *cis*-$2N_b.4O_w$ types are discussed below.

• *cis*-$2N_b.4O_w$ coordination (3 well-defined occurrences): One SSU and two LSU *cis*-$2N_b.4O_w$ patterns involving N7 atoms were observed. They involve G/G or A/G nucleotide pairs and were described elsewhere as purine N7 seats (14,27). However, it might be more appropriate to name them "head-to-tail stacked purine" motifs (**Figures 8/S3**). In each case, these ions that bind to two N7 atoms are also coordinated through water-mediated contacts to at least three OP2 atoms forming a total of 8 to 9 inner- and outer-shell contacts. This rare motif, also present in Group I intron structures, are undoubtedly involved in the folding and stabilization of the rRNA subunits and are recurrent in ribosomes from various kingdoms (14,27).

Some of us questioned earlier the nature of the ion associated with the *cis*-$2N_b.4O_w$ motif and suggested that the assigned Mg^{2+} might in fact be a hexahydrated Zn^{2+} given the very high-density peaks observed in some related X-ray structures and given that the affinity of Mg^{2+} for purine N7 atoms is much lower than that of Zn^{2+} (14,53). However, based on the present high-resolution structure, these ions are more likely Mg^{2+} in most of the known structures.

• *trans*-$2O_{ph}.4O_w$ coordination and variations (10 well-defined occurrences among 14): These patterns are less frequent than the *cis*- patterns but still significant. They appear more difficult to characterize given $d(O_{ph}\ldots O_{ph})$ ≈4.2 Å (**Figure 3**). The architecture of these patterns suggests that they are more flexible and probably slightly less stable than the patterns in *cis*- (**Figure 7C**). Variations of this motif involving the replacement of one or two O_{ph} atom(s) by O_b/N_b atoms are not observed.

• *fac*-$3O_{ph}.3O_w$ and *mer*-$3O_{ph}.3O_w$ coordination's and variations (22 well-defined occurrences among 23): The $3O_{ph}.3O_w$ arrangement comprises 7 *fac*- and 9 *mer*- arrangements. We believe these arrangements to be especially important for the ribosome structure, and especially those that join ribosomal domains. All these occurrences comprise a Mg^{2+} bidentate motif with one exception in the SSU where the bidentate motif involves an insertion of two nucleotides (**Figure 9**).

As variations of these motifs, two *mer*-$2O_{ph}.O_b.3O_w$, two *fac*-$2O_{ph}.N_b.3O_w$ and one of each *mer*-$O_{ph}.2O_b.3O_w$, *fac*-$2O_{ph}.O_r.3O_w$ and *mer*-$2O_{ph}.O_{cno}.3O_w$ binding sites were observed. Several of these motifs are associated with $Mg^{2+}\ldots K^+$ pairs (see below). Two of these motifs are inducing turns associated with three consecutive nucleotides that are probably impossible to achieve, like bidentate binding in general, without the participation of a Mg^{2+} ion.

• *Cis/Trans*-$4O_{ph}.2O_w$ coordination and variations (5 well-defined occurrences among 8): These motifs are rare given that structural architectures able to dehydrate four times a hexahydrated Mg^{2+} ion need very intricate folds that were detected only in a few specific rRNA regions. In 8B0X, we observed five well-defined such binding sites in the LSU, two poorly defined in the SSU and one poorly defined in the uS2 r-protein. For naming these binding sites, we considered the *Cis-/Trans-* placement of the two bound water molecules (note that we used capitals for *Cis-/Trans-* as a marker for these binding sites; see **Methods**). The first binding site (**Figure 10A**) is *Trans*-$4O_{ph}.2O_w$ with Mg^{2+} being coplanar to all O_{ph} atoms. It is the sole occurrence of the *Trans-* type. The second (**Figure 10B**) is *Cis*-$4O_{ph}.2O_w$. This domain V site in *Cis-* displays a unique pattern of three consecutive nucleotides wrapping around a Mg^{2+} ion. A fourth nucleotide from domain II completes this O_{ph} based patterns.

Three other well-defined sites involve O/N atoms in place of O_{ph} atoms. A *Cis*-$3O_{ph}.O_b.2O_w$ site is associated with a (U)O4 atom, a *Cis*-$3O_{ph}.O_r.2O_w$ site is associated with a rare coordinating O2' atom

(see below), a *Cis*-$2O_{ph}.O_{back}.2O_w.N_{His}$ site joins the uL3/15 r-proteins to the LSU. Additionally, three occurrences with Mg^{2+} having a density peak value < 4.0 were also characterized such as a *Cis*-$2O_{ph}.2O_b.2O_w$, a *Cis*-$3O_{coo}.2O_w.N_{His}$ and a poorly defined *Cis*-$O_{ph}.3O_{back}.2O_w$ binding site in uS2.

These intricate motifs mostly based on Mg^{2+} bidentate chelation, are rare since they require complex folding events that can only emerge in the larger RNAs. It is expected that variations of these motifs remain to be characterized in the larger and more complex eukaryotic ribosomes.

Rare inner-shell Mg^{2+} binding to O2' atoms

Binding of Mg^{2+} to O_r atoms is rare (14). No inner-shell Mg^{2+} binding to O3'/O4'/O5' atoms were observed in 8B0X. However, 3 intriguing and well-defined Mg^{2+}…O2' binding events were observed, two of which involving an intranucleotide O2'/OP1 and an O2'/OP2 bidentate contact. These two binding events are associated with a remarkable nucleotide conformation. Indeed, only two O2'…OP short contacts of the Mg^{2+}…O2'-C2'-C3'-P-OP…Mg^{2+} (or six-membered rings) were localized in the entire 70S. A Mg^{2+} is associated with each of the two instances. The first Mg^{2+} binding type is *Cis*-$3O_{ph}.O_r.2O_w$ (**Figure 11A**). This is the only 8B0X binding type where four consecutive nucleotides form inner-shell contacts. The second is *fac*-$2O_{ph}.O_r.3O_w$ and involves three consecutive nucleotides (**Figure 11B**). Both represent non-superposable examples of bidentate bindings. They involve rare backbone conformations where the first shell OP1/OP2 atoms are at 3.0/2.8 Å from the first shell O2' atom of the same residue. The third more hypothetical O2' contact of the $O_r.5O_w$ type is described in **Figure S2C**. Overall, these three occurrences imply that in the right context, O2' atoms can be part of the Mg^{2+} first coordination shell.

Anionic base pairs in 8B0X

Next, we describe a few peculiarities of the 8B0X structure. According to a recent study (66), four anionic base pairs are present in 8B0X and in bacterial ribosomes in general. Two in the SSU and one in the LSU are related to U(-)•G pairs (**Figure 12**). A fourth LSU instance is a cWW G•G(-) pair. Two of these pairs are associated with a Mg^{2+} ion (**Figure 12**). These base pairs involve a deprotonated uridine/guanine that carry a negative charge leading to U(-)•G and G•G(-) pairs.

One of these U(-)•G pairs is connected to a Mg^{2+} ion and displays a unique Mg^{2+} binding pattern of the *mer*-$O_{ph}.2O_b.3O_w$ type with all but two water molecules being coplanar. These features related to negatively charged U(-)/G(-) nucleobases are unique in the ribosomal ecosystem. We also note the occurrence of an [A^+•C]•ho5C base triple (**Figure S4**) associated with the ho5C base modification that benefits *E. coli* under oxidative stress conditions (67).

Unexplained "metal" binding patterns

While in 8B0X most well-ordered ion binding sites could be assigned to Mg^{2+}/K^+ ions, two sites associated with peaks suggesting the presence of a solvent particle with ≈2.07 Å coordination distances could not be linked to one of these ions. However, the definition of the associated density patterns entrusts their examination (**Figure 13**).

In the SSU, a solvent particle links the two N7 atoms of a potential ion-mediated A…G pair (**Figure 13A**). This solvent density with a peak at ≈2.1 Å from the two N7 atoms could only be occupied by an

undetermined tetrahedral ion. Hence, we placed a UNX ion with a $2N_b.2O_w$ coordination in our model, UNX being the PDB code for an unknown atom/ion.

In the LSU, an even stranger A…G pair is observed. A density peak occurs between the (A)N1 and the (G)N7 atoms with the A and G bases being strictly coplanar (**Figure 13B**). This pattern resembles that of metal mediated base pairs (**Figure S5**) containing Ag, Hg or Au ions (68-71). To the best of our knowledge, such an ion mediated base pair has not been observed in the 7K00, 8FTO and 8CGK *E. coli* ribosomes. In the later structures, the adenine is shifted to establish a (A)N6…N7(G) hydrogen bond (**Figure S5**). We also placed an UNX ion at this position.

These observations hint to the presence of metal contaminants in 8B0X that are not present in other ribosomal structures and that are difficult to identify through conventional techniques (72). Indeed, the inclusion of molecules not added to the buffer can be observed in cryo-EM structures as is the case for two polyamines mentioned in a recent 1.9 Å resolution *Human* 80S structure (73).

Mg^{2+}…Mg^{2+} ion pairs

An intriguing feature of the rRNA ionic shell is related to the occurrence of Mg^{2+}…Mg^{2+}, Mg^{2+}…K^+ and K^+…K^+ ion pairs although ion pairs have been discussed in other nucleic acid and protein systems (61,74-76). An ion pair is formed when two metals share at least one and up to three phosphate groups, oxygen atoms or water molecules. In 8B0X, none of these pairs are associated with r-proteins and the involved Mg^{2+} ions are hexacoordinated. We propose a preliminary classification of these pairs, although their limited occurrence in 8B0X suggest that more configurations remain to be uncovered through the exploration of other ribosomes and RNA systems. At the present stage, we divided the observed Mg^{2+}…Mg^{2+} pairs into four categories, the last one being speculative. The group I involves Mg^{2+} ions that are separated by > 4.5 Å and contact a same phosphate group. The group II/III/IV display inter-metal distances in the 2.4–3.8 Å range. In these groups, the metals can share one and up to three oxygen atoms from water molecules and phosphate groups belonging to their first coordination shell. Note that the net charge on the Mg^{2+} ions might significantly decrease in such configurations (61).

• Group I or "Magnesium micro-clusters" (Mg^{2+}-μc): Mg^{2+}…OP-P-OP…Mg^{2+} with $d(Mg^{2+}…Mg^{2+})$ ≈4.5–5.3 Å (17 well-defined occurrences). The Mg^{2+} ions share one or two phosphate group, but no water molecules given the large inter-metal distance > 4.5 Å (**Figure 14A/S6A**). These arrangements were called Mg^{2+}-μc by Williams and co-workers (1,5,48,77) and resemble the bridges formed by carboxylate groups between two metal ions in enzymatic systems (61). In rRNA, such Mg^{2+}-μc's were considered to be part of the peptidyl transferase center of various ribosomes from a large range of species and were also found in the P4-P6 domain of the tetrahymena group I intron ribozyme (78) and the self-spliced group II intron from *Oceanobacillus iheyensis* (79) among other structures. These arrangements forming up to five inner-shell contacts are essential for the folding of the rRNA core as are the Mg-μc's described in (1,5,48,77). Most of the ion pairs share a common phosphate group while only two of them share two common phosphate groups (**Figure 14A**). Therefore, we propose to categorize these Mg^{2+}-μc into three types. When each Mg^{2+} is coordinated to two phosphate oxygens the micro-cluster is Mg^{2+}-$μc_{22}$, when only one Mg^{2+} is coordinated to two phosphate oxygens it is Mg^{2+}-$μc_{21}$ and when only one phosphate group is involved, it becomes Mg^{2+}-$μc_{11}$ (**Figure S7**).

Arrangements where three Mg^{2+} ions are linked by two phosphate groups are located at the LSU/uL2 interface (**Figure 15**). Overall, these configurations show the intricacy of Mg^{2+} binding motifs that can assemble to form more complex patterns such as those observed in the rRNA core at various locations that form extended chains of Mg^{2+}/K^{+} ions connected by water and phosphate groups.

• Group II: $Mg^{2+}\ldots O_w\ldots Mg^{2+}$ with $d(Mg^{2+}\ldots Mg^{2+})$ ≈3.8 Å (2 well-defined occurrences). In the 1st pair, the ions share a single water molecule and no RNA atoms (**Figure 14B**). The 2nd pair involves one shared water molecule. In addition, two Mg^{2+} connected waters are separated by 2.07 Å suggesting the presence of an alternate conformation that must be interpreted with caution (**Figure S6B**).

• Group III: $Mg^{2+}\ldots O_w\ldots Mg^{2+}$ with $d(Mg^{2+}\ldots Mg^{2+})$ ≈2.8 Å (2 well-defined occurrences). Both ions of a 1st pair share an OP1 atom and two water molecules (**Figure 14C**) while the two ions of a 2nd pair share three water molecules (**Figure S6C**). These instances recall a documented example of an $Mg^{2+}\ldots Mg^{2+}$ ion pair where the ions are separated by 2.7 Å (76). This pair appears in a structure of a 5S rRNA Loop E fragment at 1.5 Å resolution (**Figure S6D**). Earlier, we proposed that such an arrangement resulted from alternate conformations of two slightly offset Mg^{2+} binding patterns (41). However, considering the two identified group III pairs in 8B0X, we re-examined this hypothesis. It seems that in specific environments, $d(Mg^{2+}\ldots Mg^{2+})$ ≈2.8 Å distances are stable. This is supported by a recent CSD structure containing a Mg^{2+} pair (80), by the description of inorganic compounds involving stable Mg(I)…Mg(I) covalent bonds with $d(Mg^{+}\ldots Mg^{+})$ ≈2.8 Å and by the implication of Mg pairs in enzymatic systems (81,82).

• Group IV: $Mg^{2+}\ldots O_w\ldots Mg^{2+}$ with $d(Mg^{2+}\ldots Mg^{2+})$ = 2.38 Å (1 well-defined occurrence). In this unique arrangement, the proximity of the two Mg^{2+} ions is astonishing (**Figure 14D**). This ion pair that involves three bridging water molecules that display surprisingly well-defined density patterns resembles the one described above (**Figures S6E/F**). The first Mg^{2+} is of the *cis*-$2O_{ph}4O_w$ type; the second involves a deformed coordination octahedron. Since, it is to the best of our knowledge the sole observation of such an ion pair in RNA, its existence needs to be confirmed through further independent observations. A rare Mg pair with $d(Mg^{2+}\ldots Mg^{2+})$ ≈2.42 Å has been described based on a 1.52 Å resolution nuclease structure, although one of the ions is not hexacoordinated (83).

$Mg^{2+}\ldots K^{+}$ ion pairs (28 well-defined occurrences among 42):

Given the exceptional 8B0X resolution, over 200 binding occurrences of K^{+} ions to rRNA atoms were observed. Among those, we identified 28 well-defined $Mg^{2+}\ldots K^{+}$ pairs with $d(Mg^{2+}\ldots K^{+})$ ≈3.5–4.4 Å. In many instances, the K^{+} ion shares two Mg^{2+} water molecules (**Figure 16A**). A subcategory of these pairs involves 10 occurrences of a K^{+} ion bound to the deep groove of G•U pairs. Seven of these pairs involve a Mg^{2+} of the $6O_w$ type. A less frequent pattern where three oxygen atoms are common to both hydration shells and associated with a shorter inter-metal distance is also observed (**Figure 16B**). In all instances, the K^{+} density peak is significantly higher than that of the Mg^{2+} ion and of their surrounding water molecules (**Figure S8**). This suggests that examining the peak heights of solvent molecules in cryo-EM structures has some value, especially when the Mg^{2+}/K^{+} ions are close in space.

The ion pairs described above are certainly common to all ribosome structures for which similar stabilization buffers were used. The question remains as to the importance of such motifs in *in vivo*

conditions where probably less divalent ions are present and where polyamines along with other metabolites contribute to the ribosome stabilization.

Mg^{2+} ions are rarely present at the SSU/LSU interface

Among all the Mg^{2+} ions identified in 8B0X, Mg^{2+} ions forming contacts to both subunits were not identified except for a single $O_{ph}.5O_w$ Mg^{2+} ion (**Figure S2A**). This suggest that Mg^{2+} ions are rarely present at the SSU/LSU interface and therefore not of structural or functional importance for the assembly of the two subunits. The presence of the single Mg^{2+} ion observed at this interface might result from the high ionic pressure imposed by the *in vitro* when compared to *in vivo* conditions and needs to be confirmed/infirmed by an examination of other high-resolution structures. This suggests that destabilization of the 70S particles observed at low Mg^{2+} concentrations might be the result of the destabilization of each of the subunits leading to more fuzzy structural interfaces rather than to paucity of divalent ions at the interface (6,84).

Mg^{2+} bound to r-proteins are few

Only one poorly defined and distorted *cis*-$3O_{coo}.2O_w.N_{His}$ binding site buried in uS2 was observed (**Figure S2B**). This binding site is also observed in the parent 8FTO structure with a better density. No other r-protein binding site was noted suggesting that r-proteins might have evolved to not compete for Mg^{2+} resources with rRNA. Overall, the need for Mg^{2+} to support proper r-protein functions is significantly smaller than that for nucleic acids.

Mg^{2+} bound at the rRNA/r-protein interfaces

A significant number of Mg^{2+} to r-protein contacts are observed at the rRNA/r-protein interfaces (**Table S1** and **SI**). Only five of these ions make direct contacts to both rRNA and r-proteins. In addition, some Mg^{2+} are forming at least one contact to the rRNA and establish water-mediated contacts to rProteins. Eight ions are located at the LSU/uL2 interface that gathers the largest number of contacts (77). This region is part of the peptidyl transferase center (PTC) that exhibit already a high number of Mg^{2+} binding sites (9,48). Petrov *et al.* noted the conservation of a Mg^{2+}-μc (**Figure 15**) at the LSU/uL2 interface that involves a N-terminal 18 amino acid loop. This interface is conserved in archaea, bacteria and eukarya (77). They discussed the importance of an Ala-Met-Asn sequence in the ribosomal assembly process. A more detailed discussion of the rRNA/r-protein interfaces is beyond the scope of this paper.

Mg^{2+} linking intra-subunit ribosomal domains

It has been made clear in several instances that Mg^{2+} ions can link ribosomal domains either through direct- or water-mediated contacts. Some of these contacts involving Mg^{2+}-μc's were described in Ref. (5,48). Several of the patterns described above are associated with inter-subunit links as illustrated in **Figures 7/9/10/11/14/15**. For defining the SSU/LSU domains and for the sake of simplicity, we used the nomenclature developed by Noller (85) and not that developed by Williams that integrates a domain "0" and "A" for the LSU and the SSU; respectively (1,86). In 8B0X, we identified 19 well-defined occurrences out of 20 where a Mg^{2+} ion makes inner-shell contacts to at least two different LSU domains and noted that inter-domain contacts are not observed in the SSU (**Table 2**). Among the former, 7 of them link LSU domain II to V, none involve domain VI and only 2 involve domain III. This suggest that

the concomitant binding of domain II to V as well as the interaction between domain V and r-protein uS2 are important Mg^{2+} dependent biogenesis steps (**Figure 15**).

A universal set of rules to characterize Mg^{2+} binding sites

One of the most important outcomes of this work is related to the straightforward binding rules we could derive from the examination of the 8B0X system and of its amended structure. A subset of these rules related to O_b/N_b atoms was described elsewhere (14,15). Here, these rules were expanded to O_{ph} atoms that represent, besides water oxygen atoms, the most important Mg^{2+} coordinating atoms. In the following, we describe these rules step by step starting by those related to the detection of the most critical Mg^{2+} bidentate motifs.

Locating Mg^{2+} bidentate clamps (O_{ph}…O_{ph}): A unique feature of Mg^{2+} binding clamps is associated with a conserved O_{ph}…O_{ph} distance close to ≈2.9±0.2 Å. This distance strictly matches that separating Mg^{2+} water molecules in *cis*- (see **Figures 3/7/9/10/11/14**). Thus, we hypothesized that a simple way to locate Mg^{2+} ions bidentate clamps was to identify all O_{ph} pairs with d(O_{ph}…O_{ph}) < 3.4 Å. By discarding the often poorly modelled pairs comprising at least one OP1/OP2 atom with B-factors > 60 $Å^2$, we located a total of 94 pairs (87 well-defined ones) comprising 36 OP1…OP1, 23 OP2….OP2 and 35 OP1…OP2 combinations. We observed that all uncovered 94 pairs were involved in Mg^{2+} binding motifs, 92 of them forming Mg^{2+} bidentate clamps. The two remaining motifs display a binding pattern involving a distinctive Mg^{2+} water-mediated contact stabilizing the short d(O_{ph}…O_{ph}) ≈2.9 Å distance (**Figure S9**). We propose that one of these binding configurations could correspond to an intermediate in the formation of Mg^{2+} bidentate clamps (**Figure S9B**).

Thus, we infer that all bidentate clamps involving Mg^{2+} can be detected in rRNA fragments of appropriate resolution by collecting O_{ph}…O_{ph} distances ≤ 3.4 Å. Of course, all higher order folding patterns of the *fac-/mer-/Cis-/Trans-* type can also be localized by checking these distances since most of them involve at least one Mg^{2+} bidentate clamps. Overall, the 94 uncovered clamps involve a limited number of 68 well-defined Mg^{2+} that are associated with essential rRNA folding patterns.

To underline the effectiveness of this rule, we stress that by just checking the O_{ph} pairs with d(O_{ph}…O_{ph}) ≤ 3.4 Å, we could identify at least 7 new Mg^{2+} bidentate clamps not assigned in the initial 8B0X structure. This illustrates the ability of this process to assign Mg^{2+} sites that escaped to the experimentalist's attention and suggests that this criterion is universal and can be applied to the search of essential Mg^{2+} binding sites in all RNA systems.

Locating $2O_b.4O_w$ and $O_{ph}.O_b/N_b.4O_w$ motifs: The $2O_b.4O_w$ binding type is rare. We found just one poorly defined occurrence involving distant residues. Similarly, we found only two well-defined $O_{ph}.4O_w.N_{His}$ occurrences involving r-protein N_{His} atoms and no $O_{ph}.N_b.4O_w$ binding types. Yet, the slightly more frequent $O_{ph}.O_b.4O_w$ binding types can be located by monitoring d(O_{ph}…O_b) ≤ 3.4 Å that can also be of the intra-nucleotide type.

Locating $2N_b.4O_w$ motifs: In most instances, although the stacking distance between two consecutive nucleotides is ≈3.4 Å, the distance between two stacked purine N7 atoms is often > 3.8 Å, therefore excluding a bidentate binding to a Mg^{2+} ion. We found that in 8B0X the only nucleobase arrangement where N7 atoms are separated by less than 3.4 Å are analogous to the ones shown **Figures 8/S3**. Indeed, only three "head-to-tail purine stacks" were detected in 8B0X and all bind Mg^{2+} ions and not

Zn^{2+} as suggested elsewhere (15). Therefore, it seems unnecessary to search for *cis*-$2N_b.4O_w$ binding types involving sequence consecutive purines.

Locating Mg^{2+} of the $O_{ph}/O_b/N_b.5O_w$ type: Locating these binding types is more difficult but the coordination geometry of the Mg^{2+} ions provides some hints as shown in **Figure 6B** and (14,15). For $O_{ph}.5O_w$, the Mg^{2+} ion must be roughly in the OP-P-OP plane and the P-OP…Mg^{2+} angle must be in the 120–160° range. For the $O_b/N_b.5O_w$ variants, the Mg^{2+} ion must be in the nucleobase plane. Yet the angle constrains are slightly different. The average (C=O…Mg^{2+}) angle is ≈144° and the ion is roughly in the alignment of one of the O_b lone pairs as confirmed by recent simulation data (46) while for $N_b.5O_w$ types the Mg^{2+} is located in the alignment of the N7 lone pair.

Locating Mg^{2+} of the $6O_w$ type: Defining binding rules for the less tightly bound $6O_w$ ions is challenging. Like for $O_{ph}/O_b/N_b.5O_w$, the Mg^{2+} ions of the $6O_w$ type that bind sufficiently strongly to the rRNA to be characterized are for most of them those that establish a high number of water-mediated contacts. Some of these binding sites represent important folding “wedges” in the structure (**Figure 5A**). The fact that these Mg^{2+} ions use their first shell water molecules to bind to appropriate rRNA binding sites such as the guanine O6/N7 and the OP1/OP2 atoms recommends scanning the rRNA hydration shell to locate potential $6O_w$ binding sites. Indeed, a precise knowledge of the rRNA hydration shell as the ones derived from experimental structures and MD simulations for protein and DNA systems will be helpful to locate the most important water-mediated Mg^{2+} binding spots (34,87-90).

DISCUSSION

Stereochemistry is an efficient tool to assign Mg^{2+} ions

Through this work we enriched the 8B0X structure by revising and completing its solvation shell and by correcting minor modelling issues. This updated structure provides insights that could not be derived with the same level of perceptiveness from lower resolution structures. Our findings are summarized in a schematic that depicts the Mg^{2+} binding types and occurrences as observed in the amended 8B0X structure (**Figure 4**). We confirmed Mg^{2+} binding patterns already discussed in earlier work (9,14,15,27) and added a full description of Mg^{2+} binding to O_{ph} atoms (9,14,15,27). We also described several ion pair types and showed how they "assemble" to form ionic chains (**Figure 15**). The characterisation of intricate ion pairs might provide an understanding of the formation of such motifs in RNA, other biopolymers and their catalytic sites (74,91-95). We also described binding patterns that could not be easily rationalized, some of them being related to metal-mediated pairs possibly involving the participation of a transition metal present in the structure as a contaminant (**Figure 14**).

Besides a thorough classification of ion binding motifs, the most important result of this study is related to the description of effective Mg^{2+} binding principles based on stereochemistry that surprise by their simplicity. In short, Mg^{2+} induces folding patterns where rRNA oxygen atoms are separated by less than 3.4 Å (**Figure 4**). By considering this principle, we observed that in every instance where $d(O_{ph}\ldots O_{ph}) \leq 3.4$ Å, the two O_{ph} atoms are for most of them bridged by a Mg^{2+} through inner-shell contacts or for two of them through inner- and outer-shell contacts (**Figure S9**). Hence, we infer that in all instances, a Mg^{2+} ion is necessary to stabilize configurations with short inter-OP distances. Indeed, given the proximity of 2 to 4 O_{ph} atoms, these are the foremost electronegative spots in ribosomes. The stabilization of such configurations can difficultly be fulfilled by K^{+} that has a much smaller charge density.

We estimate that distance criteria reach close to 100% efficiency in the detection of bidentate binding sites for the present structure, a percentage that needs to be confirmed by scanning a larger variety of ribosomal and other RNA structures and is certainly affected by local resolution. In that respect identifying binding sites by using stereochemical rules might have an edge over those that are solely based on electrostatic potentials (1).

For characterizing the $O_{ph}.5O_w$ and $6O_w$ binding sites, stereochemical considerations that involve a correspondence between the Mg^{2+} hydration shell and that of local rRNA folds associated with the guanine Hoogsteen edge, among other sites, are determining (**Figure 4/5**). Overall, the analysis of this system illustrates the principle of water molecules mediating contacts between a biopolymer and a ligand that has recently been addressed for ribosome/drug interfaces (38). The replacement of rRNA bound water molecules by Mg^{2+} first shell waters illustrates a rational drug-design strategy that needs high-resolution structures to develop (96,97).

The most intricate ion binding pockets described above correspond to emerging motifs that cannot be formed by smaller biopolymers and are for most of them embedded in the core of the ribosome structure during biogenesis, the role of ions on this process having not yet been addressed (98,99). Thus, Mg^{2+} stabilizes distinctive conformational and energetic states by sharing a special geometric and electrostatic complementarity. We suggest that the stereochemically based binding rules we

defined are universal for RNA and might also apply to DNA and protein systems. There is little doubt that variations of the uncovered binding motifs will continue to be characterized with additional high-resolution structures. However, we trust that instances of all essential Mg^{2+} binding sites were described for this bacterial ribosome including two novel and intriguing binding patterns involving O2' atoms.

In turn, this suggests that besides the classical and well-described RNA motifs ranging from tetraloops to kink-turns, other motifs must be considered in the assembly of large RNAs. In this study we described a few novel motifs where up to five adjacent nucleotides wrap around a single ion. Indeed, the apparently simple classification we propose for Mg^{2+} binding underlines a large variety of motifs if one considers the combinatorial possibilities associated with the nature and relative positions of the coordinating atoms. The motifs and principles described in this study will certainly benefit groups involved in RNA folding competitions such as RNA-puzzle (100,101). The techniques that are currently used for folding an RNA from its sequence rarely use information related to water or to the RNA ionic shell.

Considerations related to ionic conditions

As stated in the method section, the final cryo-EM buffer contains 25 mM $Mg(OAc)_2$ and 100 mM K(OAc). Yet, some studies suggested that optimal buffer conditions for functional ribosomes are in the 2–5 mM range for Mg^{2+}, in the 60–150 mM range for K^+ when 2 mM of spermidine are present (2). Although the total Mg^{2+} concentration in the cell is in the 17–20 mM range which is close to the 25 mM cryo-EM buffer condition, it has been reported that the concentration of non-chelated hexahydrated Mg^{2+} ions in a crowded intracellular environment is in the 1–2 mM range (102). Thus, it is possible that the excellent 1.55 Å resolution of the 8B0X structure is a byproduct of this high 25 mM Mg^{2+} concentration that might have (over)saturated Mg^{2+} binding sites. Hence, one can wonder if under such a high Mg^{2+} pressure, the number of Mg^{2+} ions observed in 8B0X exceeds those necessary for a ribosome to perform its *in vivo* tasks (16,84,103) and might have favoured the formation of some of the ion pairs we described.

At Interestingly, the addition of weakly chelating agents to buffers was found to enhance RNA function including thermodynamic and chemical stability as well as catalytic efficiency probably by sequestering an excess of divalent ions that would have adverse structural and functional effects (102,104,105). Alike, the "goldilocks" theory affirms that for some systems, a low Mg^{2+} concentration affects RNA properties by preventing suitable folding whereas a too high Mg^{2+} concentration might reduce activity (103). In line with these conjectures, it has been shown that excess Mg^{2+} reduces translational activity and accuracy (106) and that the error frequency measured *in vitro* at 10 mM Mg^{2+} is 10 times higher than at 5 mM Mg^{2+} in the absence of spermidine (107). Elsewhere, we speculated that an excess of Mg^{2+} might over-stabilize ribosomal structures and grip the translation machinery by binding to the mRNA and tRNAs while a less organizing ion such as K^+ would act as a lubricant favouring a smooth transition from one state to another thereby preserving an optimal turn-over rate (16).

From our survey, we infer that the optimal number of chelated Mg^{2+} comprise the ≈100 ions that are involved in the coordination of at least two non-water oxygens such as the $2O_{ph}.4O_w$ ions which are for most of them incorporated during biogenesis. A proportion that remains to be determined of the remaining ≈290 $O_{ph}.5O_w$ and $6O_w$ ions that display limited or no access to the bulk solvent might also

be integrated into the ribosome during biogenesis (**Figure 5A/6A**). Thus, it is not known if the ≈170 O_{ph}.5O_w ions are all essential for ribosome activity or are the result of an excess of Mg^{2+} ions in the cryo-EM buffer. The same reasoning holds for the 115 assigned 6O_w ions and the exact balance of monovalent and divalent ions under both *in vivo* and cryo-EM conditions is not precisely known.

To summarize, we along with the authors of the 8B0X structure were able to characterize the to date largest amount of site bound Mg^{2+}/K^+ ions for a ribosome thanks to a thorough analysis of this structure at an exceptional 1.55 Å resolution. Nevertheless, the 634 Mg^{2+}/K^+ ions we could model carry a total of ≈1,040 positive charges. This is far from being sufficient to neutralize the ≈5,000 nucleotides of this structure even if we take into account the ≈525 excess positive charges carried by all the bound r-proteins or the ≈1,160 charges carried by all the positively charged Lys/Arg residues they embed. For finding the "missing" ions accounting for the neutralization of the remaining ≈3,000 positive charges, other methods will have to be used such as MD simulations that are currently the only available techniques able to describe the diffuse binding of ions such as K^+ and $Mg(H_2O)_6^{2+}$.

Amending existing structures

This study also raises the issue of amending existing PDB structures, a practice that should be better integrated in the habits of the structural community (18). It is clear that the 8B0X refinement process was not conducted to its end regarding the solvation shell. That's understandable given the amount of time needed to conduct such a task. Yet, we have to consider that structures deposited to the PDB are a timely interpretation of the experimental data that can be corrected for flaws or omissions by using knowledge acquired after their deposition (22,108,109). A nice illustration of this process is provided by the multiple corrections brought to the original *Haloarcula marismortui* 50S structure first deposited to the PDB in 2000 with its last refinement deposited in 2013 (8,13). In the present case, we were able to produce significant improvements to the bacterial ribosomal ionic structure as deposited to the PDB with the 8B0X identification code and suggest that a large subset of PDB structures can be amended by using strategies similar to those described in this paper

CONCLUSIONS

We believe that the Mg^{2+} binding principles we uncovered through a careful analysis of the 8B0X bacterial ribosome and its amended structure combined with a thoughtful consideration of stereochemical rules will allow to develop more precise and automatized strategies to rapidly complete the ionic shell of small and large RNAs that involve or not AI strategies. We also believe that we have provided a complete description of all the major Mg^{2+} chelation sites that involve at least 2 and up to 4 non-water coordinating atoms. This description of intricate Mg^{2+} binding motifs also comprising that of ion pairs will enrich the ways we use to think and talk about RNA folding, structure and catalysis of these large systems (110).

SUPPLEMENTARY DATA

Supplementary Data are available at NAR online.

ACKNOWLEDGEMENT

P.A. wishes to thank Dr Yaser Hashem and Dr Quentin Vicens for comments on the manuscript and Dr Nawavi Naleem for computational assistance.

FUNDING

S.K. and A.H.K are supported by NYUAD AD181 faculty research grant and REF Grant RE317.

CONFLICT OF INTEREST

None

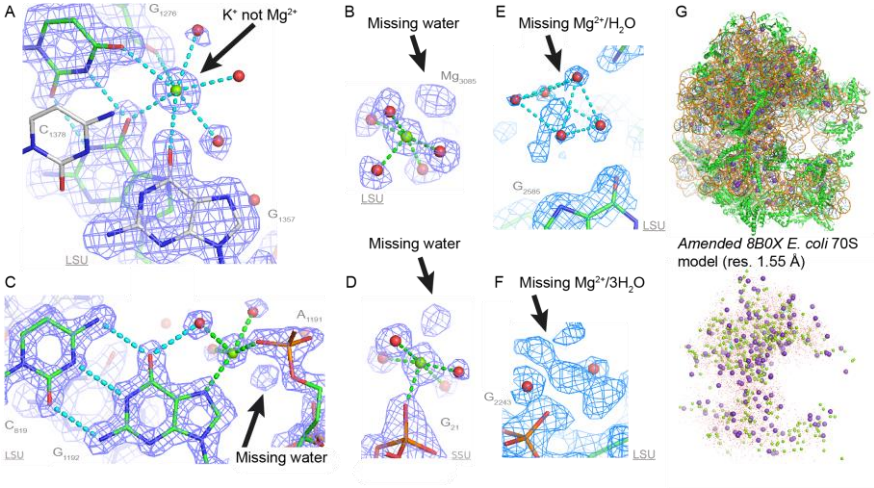

Figure 1. Examples of 8B0X ion assignments and first shell completion issues. (**A**) The Mg^{2+} ion has been placed in the deep grove of a G•U pair (a neighbouring C=G pair is shown with silver carbons). The ion heptahedral coordination and the *d*(Mg^{2+}…O) ≈2.8 Å distances imply that this ion is K^+ and not Mg^{2+}. (**B**) The $6O_w$, (**C**) $O_{ph}.N_b.4O_w$ and (**D**) $O_{ph}.5O_w$ magnesium ions display missing first shell water molecules. Defining a correct ion binding type in the absence of these water molecules is challenging. (**E**) A Mg^{2+} and a water molecule belonging to a hexahydrated Mg^{2+} were not assigned. This Mg^{2+} binds to a guanine Hoogsteen edge. (**F**) The densities of the ion and of three water molecules belonging to a Mg^{2+} of the $O_{ph}.5O_w$ type were left empty. The lines in green and cyan correspond to distances below 2.3 Å and in the 2.6–3.2 Å range, respectively. (**G**) View of our amended 8B0X model (top) and of its solvation shell with 403 Mg^{2+}, 231 K^+ and 21.397 water molecules shown by green and purple spheres and by red dots, respectively (bottom).

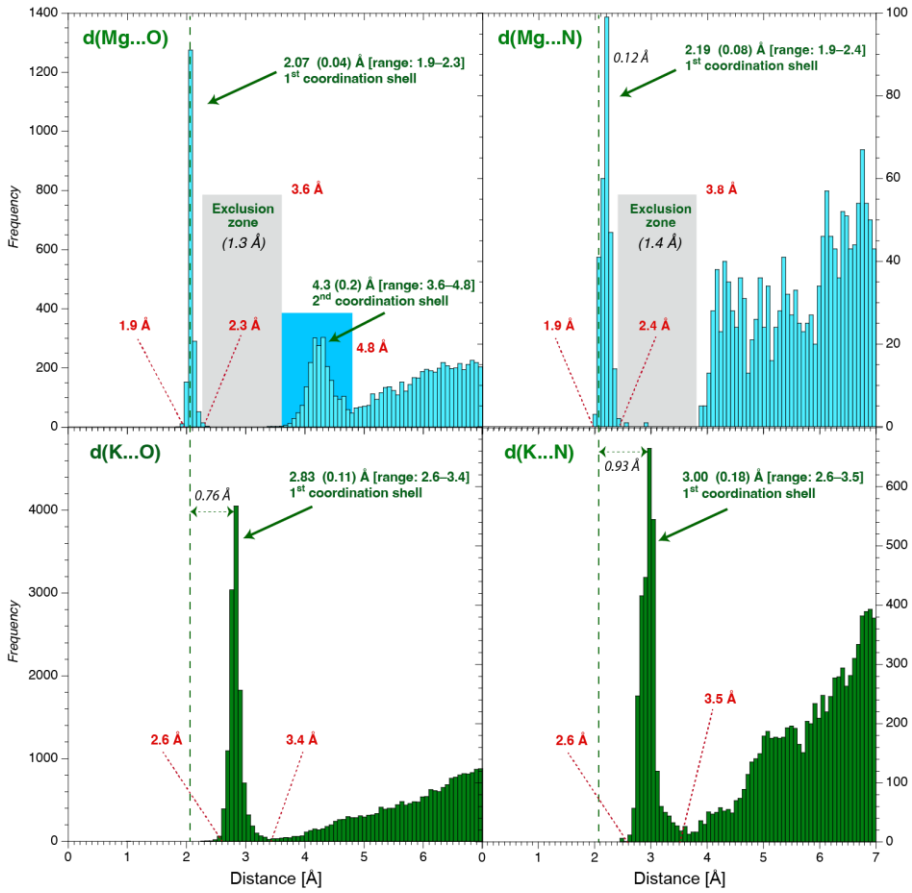

Figure 2. O/N coordination distance histograms for Mg/K derived from the CSD (version 5.43, update November 2022). (**Top**) See the **Method** section for a description of the criteria used for the CSD searches. Mg ions were considered as hexacoordinated; no coordination number constraints were placed on K. Standard deviations for the 1st and 2nd peaks are in parenthesis. All types of O and non-protonated N atoms were used to build these histograms (14,15,53). A vertical dashed line marks the average *d*(Mg…O) ≈2.07 Å coordination distance in all histograms. Mg exclusion zones are marked by grey rectangles.

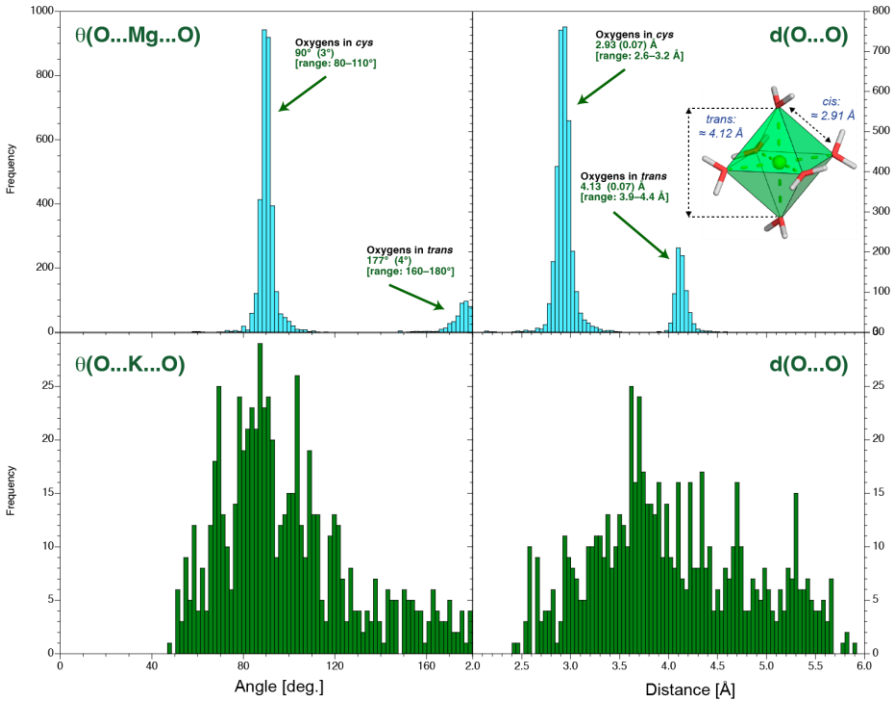

Figure 3. First shell oxygen coordination angle and distance histograms for Mg/K derived from the CSD. (**Left**) Coordination angle histograms for θ(O…Mg/K…O) and (**right**) related coordination distances for oxygen ligands in the ion first coordination shell derived from the CSD (51,52). The insert shows an ultra-high-accuracy X-ray structure of $Mg(H_2O)_6^{2+}$ that illustrates the octahedral arrangement of water molecules in the Mg^{2+} first hydration shell (111,112) and emphasizes the *cis-/trans-* binding patterns. The angle histograms for K are not very useful given that the most frequent K ligands in the CSD are diethoxy (O-C-C-O) groups originating from crown ethers and cryptands. These groups are rare in nucleic acids except when the cryo-EM/X-ray buffers contains ethylene glycol monomers or PEG fragments (113). Diethoxy groups were excluded from the CSD searches shown **Figure 2/3**.

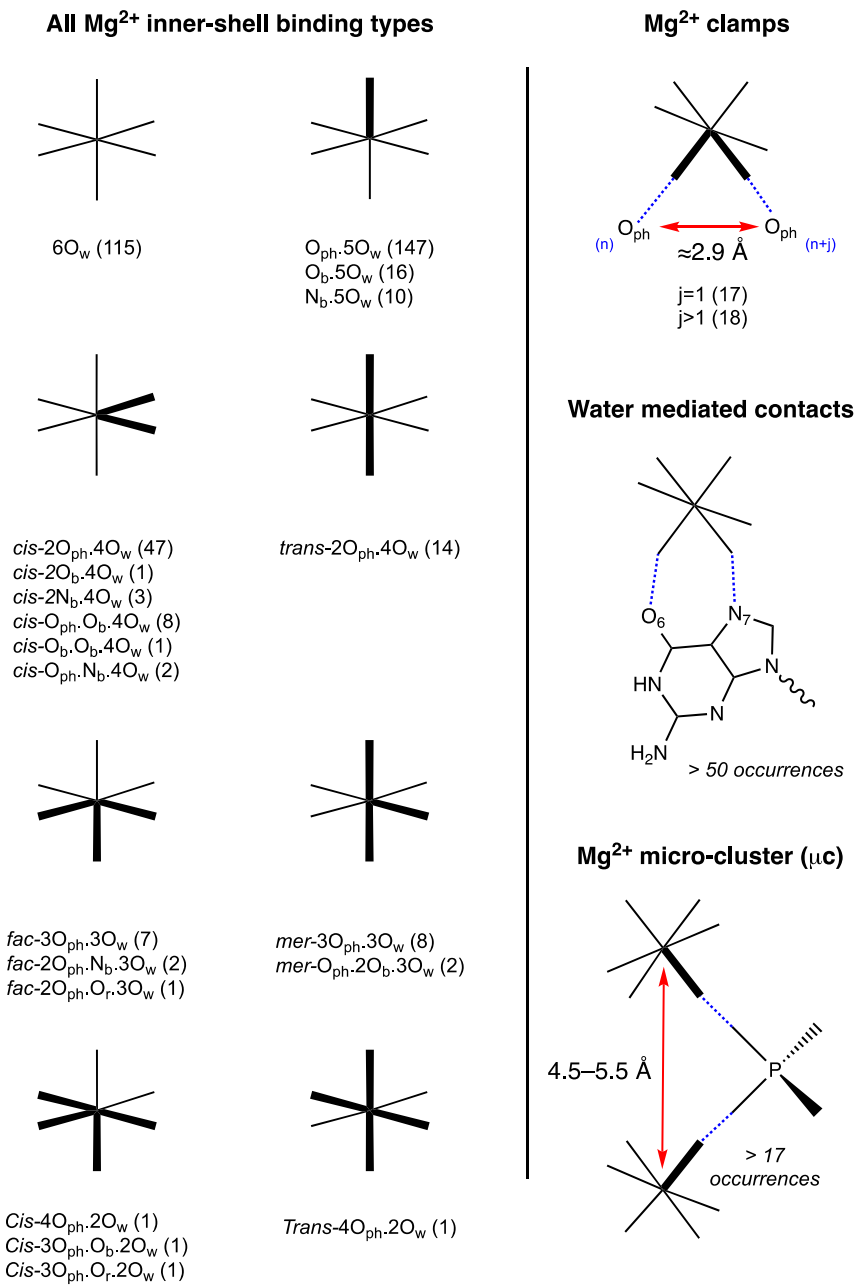

Figure 4. Schematics of Mg^{2+} binding types and occurrences as observed in the amended 8B0X structure. (Left) In addition to the outer-shell $6O_w$ binding type, all the inner-shell Mg^{2+} ion binding types and occurrences uncovered in the 8B0X structure are shown (we do not consider binding to r-proteins that account for 15 ions). (Right) The top panel shows a Mg^{2+} clamp where the ion coordinates in *cis*- to two adjacent (j=1) or distant (j>1) O_{ph} atoms. The middle panel shows a Mg^{2+} binding to a guanine Hoogsteen edge. The bottom panel shows a Mg^{2+}-μc.

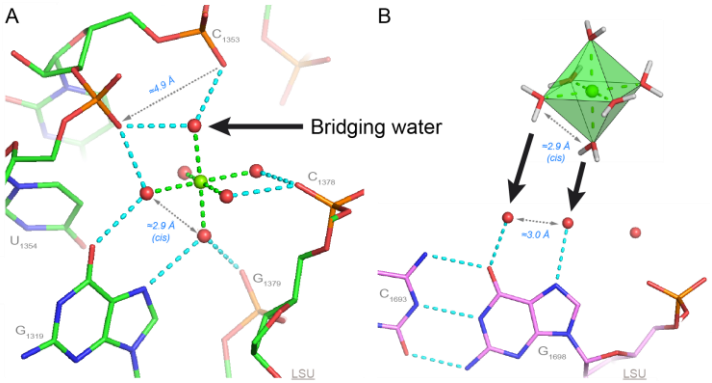

Figure 5. A 6O$_w$ Mg^{2+} ion establishing eight 2nd shell water-mediated contacts to rRNA atoms and schematics of binding of hexahydrated ions to a guanine Hoogsteen edge. (**A**) The 6O$_w$ Mg^{2+} ion occupies a tight binding pocket where it forms eight 2nd shell water-mediated contacts. Note the binding of two first shell water molecules to a guanine Hoogsteen edge and the recurrent first shell water molecule bridging two consecutive phosphate groups. (**B**) Schematics illustrating how two water molecules bound to the guanine Hoogsteen edge O6/N7 atoms and separated by ≈2.9 Å can be replaced by two first shell water molecules in *cis*- of a Mg[H$_2$O]$_6^{2+}$ ion. The lines in green and cyan correspond to distances below 2.3 Å and in the 2.6–3.2 Å range, respectively. For clarity, experimental densities and some water molecules are not shown.

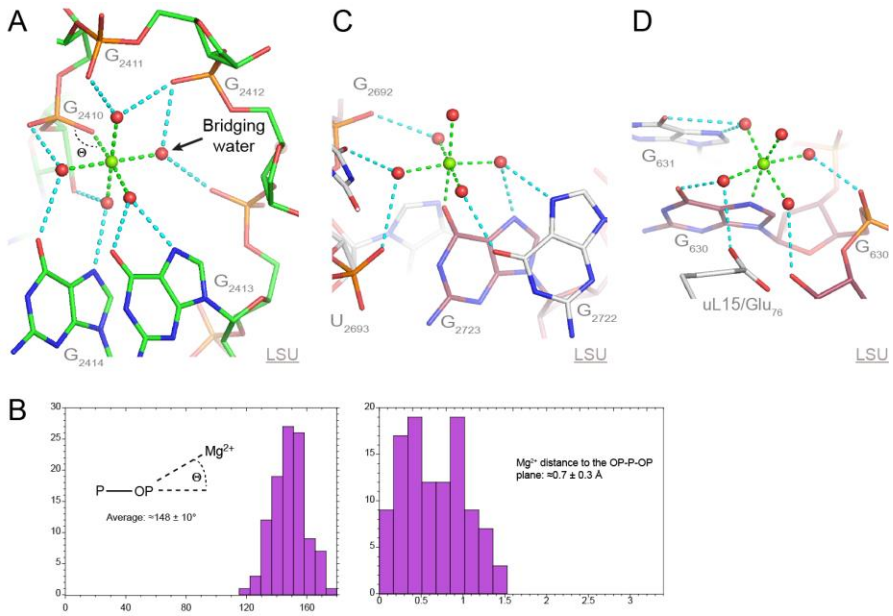

Figure 6. Examples of $O_{ph}/O_b/N_b.5O_w$ Mg^{2+} ions establishing 2nd shell water-mediated contacts to rRNA atoms. (**A**) This Mg^{2+} ion of the $O_{ph}.5O_w$ type is the most highly connected ion in 8B0X with one inner-shell and 10 outer-shell contacts. Strikingly, this Mg^{2+} establishes inner- and outer-shell contacts with five consecutive nucleotides and displays a bridging water molecule as in **Figure 5A**. (**B**) The left histogram shows the P–OP…Mg^{2+} angular distribution with the average value calculated from the ensemble of 105 well-defined $O_{ph}.5O_w$ occurrences. The right histogram describes the Mg^{2+} distance to the OP–P–OP plane for the same 105 occurrences. (**C**) This Mg^{2+} of the $O_b.5O_w$ type, although less connected, establishes inner- and outer-shell contacts to two consecutive guanine Hoogsteen edges. (**D**) This Mg^{2+} of the $N_b.5O_w$ type establishes inner- and outer-shell contacts to a guanine Hoogsteen edge and a r-protein. The lines in green and cyan correspond to distances below 2.3 Å and in the 2.6–3.2 Å range, respectively. For clarity, experimental densities and some water molecules are not shown.

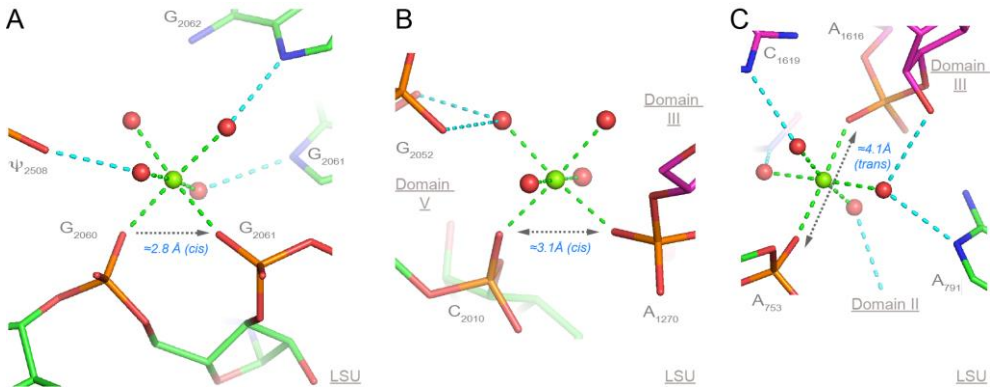

Figure 7. Two *cis*-2O$_{ph}$.4O$_{w}$ and one *trans*-2O$_{ph}$.4O$_{w}$ motifs. (**A**) The two adjacent phosphate groups form a bidentate Mg^{2+} binding motif also defined as Mg^{2+} 10-membered rings (48,64,65). (**B**) The two phosphate groups are distant in sequence and Mg^{2+} bridges domains III and V. (**C**) The two phosphate groups are in *trans*- and the associated Mg^{2+} joins LSU domains II and III. The lines in green and cyan correspond to distances below 2.3 Å and in the 2.6–3.2 Å range, respectively. For clarity, experimental densities and some water molecules are not shown.

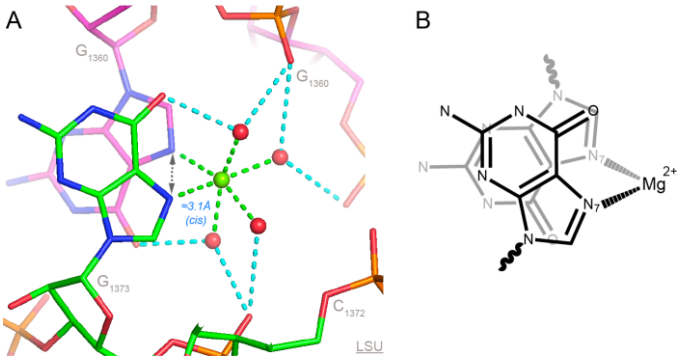

Figure 8. Example of a "head-to-tail stacked purine" motif. (**A**) Two guanines coordinate a Mg^{2+} through their N7 atoms in a *cis*-$2N_b.4O_w$ arrangement. As a result, a total of 9 inner- and outer-shell contacts are formed. The purines in these examples are separated by >10 nucleotides. Two similar *cis*-$2N_b.4O_w$ arrangements are described in (**Figure S3B/C**). The lines in green and cyan correspond to distances below 2.3 Å and in the 2.6–3.2 Å range, respectively. For clarity, experimental densities and some water molecules are not shown.

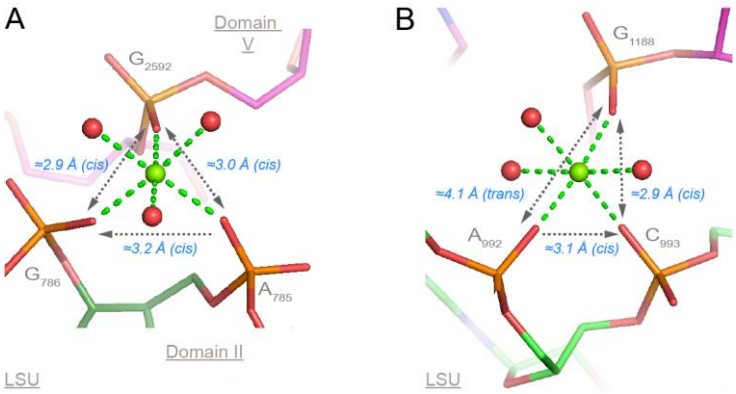

Figure 9. Examples of *fac*- and *mer*-3O$_{ph}$.3O$_{w}$ binding sites. (**A**) The Mg^{2+} is of the *fac*-3O$_{ph}$.3O$_{w}$ type. (**B**) The Mg^{2+} is of the *mer*-3O$_{ph}$.3O$_{w}$ type. In both instances, a bidentate Mg^{2+} clamp is associated with a distant phosphate group. The lines in green and cyan correspond to distances below 2.3 Å and in the 2.6–3.2 Å range, respectively. For clarity, experimental densities and some water molecules are not shown.

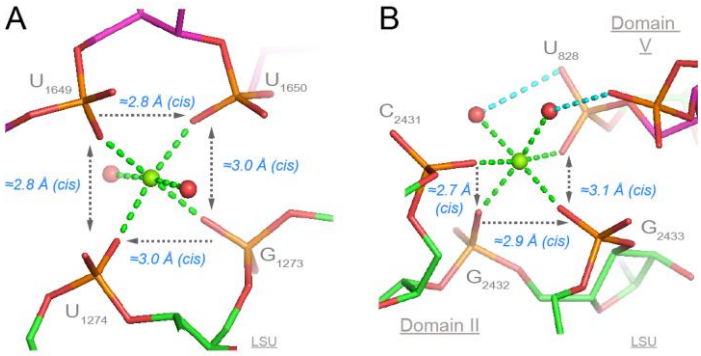

Figure 10. Example of *Trans*- and *Cis*-2O$_{ph}$.4O$_{w}$ binding sites. (**A**) This Mg^{2+} is of the *Trans*-2O$_{ph}$.4O$_{w}$ type and involves two bidentate Mg^{2+} clamps. (**B**) This Mg^{2+} is of the *Cis*-2O$_{ph}$.4O$_{w}$ type. The carbons of the domain V and II are in green and purple, respectively. The two consecutive bidentate Mg^{2+} clamps form a rare pyramid motif described in (29) that involves three adjacent nucleotides. The lines in green and cyan mark distances below 2.3 Å and in the 2.6–3.2 Å range, respectively. For clarity, experimental densities and some water molecules are not shown.

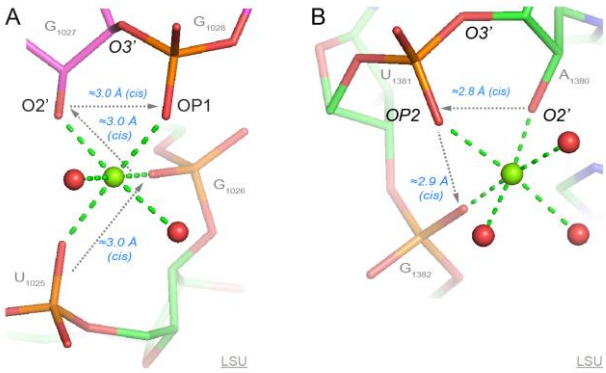

Figure 11. View of two rare Mg^{2+} binding to O2' atoms. (**A**) This Mg^{2+} is of the *Cis*-$3O_{ph}.O_r.2O_w$ type. It involves a turn formed by four consecutive nucleotides and a rare backbone conformation leading to a short (n)O2'…(n+1)OP1 distance close to 3.0 Å. (**B**) This Mg^{2+} is of the *fac*-$2O_{ph}.O_r.3O_w$ type. It involves a turn formed by three consecutive nucleotides and a rare backbone conformation leading to a short (n)O2'…(n+1)OP2 distance close to 2.8 Å. As such, the two conformations are different since they involve OP1 and OP2 atoms respectively. The lines in green and cyan correspond to distances below 2.3 Å and in the 2.6–3.2 Å range, respectively. For clarity, the experimental densities and some water molecules are not shown.

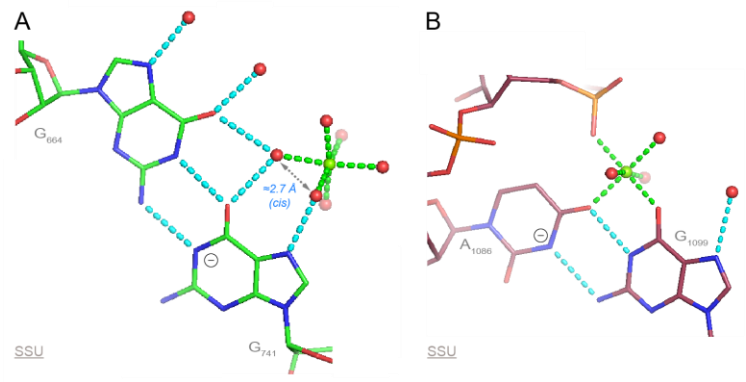

Figure 12. Two Mg^{2+} bound base pairs with a negatively charged guanine/uridine nucleobase. (**A**) The G•G(-) pair with a negatively charged guanine. The $6O_w$ Mg^{2+} binds to a Hoogsteen edge. (**B**) The U(-)•G pair with a negatively charged uridine. This base pair is associated with a unique Mg^{2+} binding pattern. The lines in green and cyan correspond to distances below 2.3 Å and in the 2.6–3.2 Å range, respectively. For clarity, experimental densities and some water molecules are not shown (see also **Figure S3**).

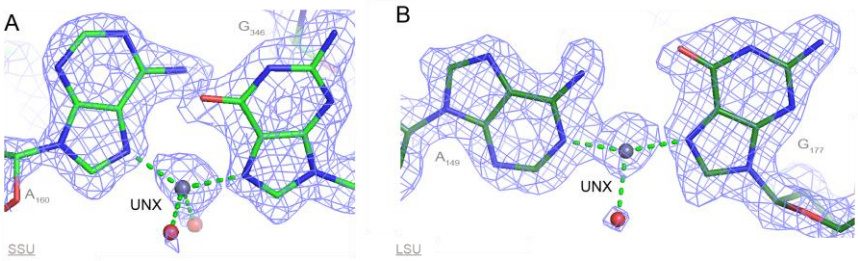

Figure 13. Unexplained ion binding patterns. (**A**) An ion mediated A…G pair. A UNX metal was placed in the density linking the two N7 atoms that was left empty in 8B0X. UNX corresponds to the PDB code for unknown atom/ion. (**B**) An ion mediated A…G pair. Similarly, a UNX ion was placed in the density linking the (A)N1 and the (G)N7 atoms that was left empty in 8B0X. The lines in green and cyan correspond to distances below 2.3 Å.

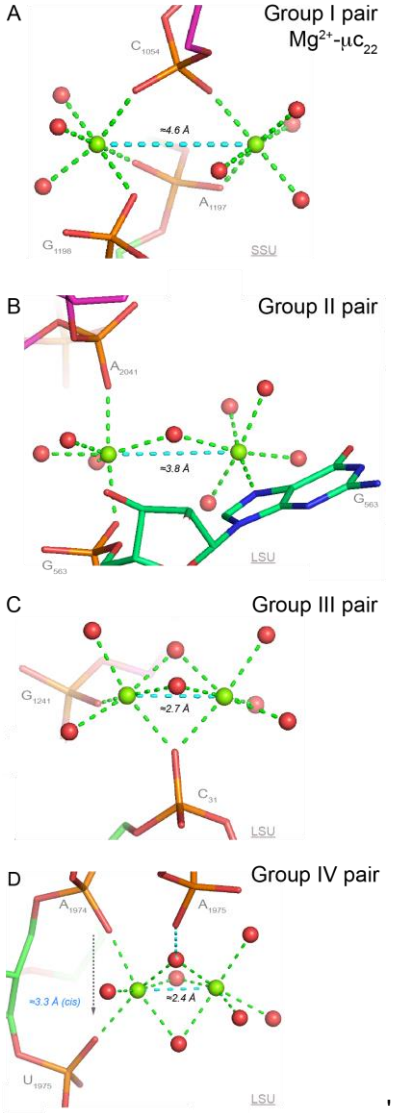

Figure 14. View of group I to IV Mg^{2+}…Mg^{2+} pairs. (**A**) The two bottom phosphate groups of this group I ion pair or Mg^{2+}-μc_{22} belong to adjacent nucleotides. The first ion is *fac*-$3O_{ph}.3O_w$, the second is *cis*-$2O_{ph}.4O_w$. (**B**) This group II ion pair joins LSU domain II and V. This pair is connected to the OP2 and N7 atoms of a same guanine and it involves a single bridging water molecule. The first ion is *trans*-$2O_{ph}.4O_w$, the second is $N_b.5O_w$. (**C**) This group III ion pair that joins LSU domain I and II involves two bridging waters and an O_{ph} atom in a regular arrangement associated with a short 2.7 Å inter-metal distance (see also **Figure S6**). The first ion is *cis*-$2O_{ph}.4O_w$, the second is $O_{ph}.5O_w$. (**D**) In the absence of corroborating examples, this group IV ion pair configuration must be considered with caution. The first *cis*-$2O_{ph}.4O_w$ ion forms a bidentate phosphate clamp, the second is $6O_w$. The dotted lines in green and cyan correspond to distances below 2.3 Å and in the 2.6–3.2 Å range, respectively. The dotted lines in orange mark the inter-metal distance. For clarity, experimental densities and some water molecules are not shown.

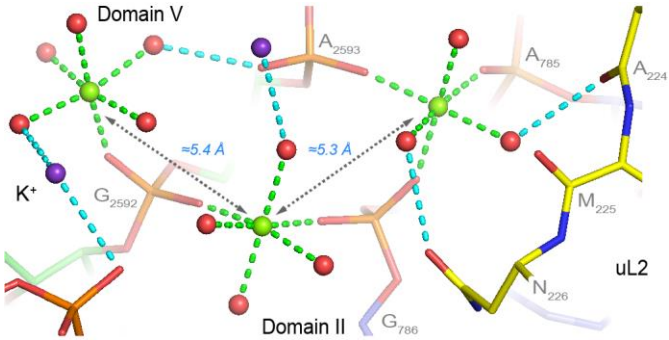

Figure 15. Partial view of the LSU/uL2 interface with a Mg^{2+}-μc. This view emphasizes the intricacy of the ion-binding patters at the LSU/uL2 interface that involves the Mg^{2+}-μc named D2 by Williams and co-workers (48,77). This Mg^{2+} binding pattern connects the domain II (right) and the domain V (left) of the LSU with a part of the N-terminal uL2 extremity (yellow backbone). From this view, it is possible to hypothesize that in a hierarchical manner, the Mg^{2+} ions help first to connect the two very distant domain II and V. When this connection is formed, uL2 can bind and the LSU approaches its functional state. Also note the presence of K^+ ions (purple spheres) at this interface. The lines in green and cyan mark distances below 2.3 Å and in the 2.6–3.2 Å range, respectively. For clarity, experimental densities and some water molecules are not shown

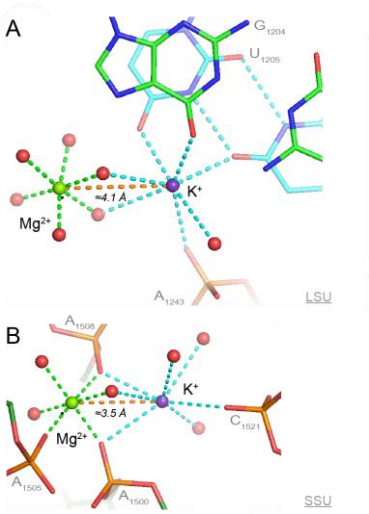

Figure 16. Two examples of Mg^{2+}…K^{+} pairs. (**A**) The first pair involves a Mg^{2+} of the $6O_w$ type and a heptacoordinated K^{+} that binds to the deep groove of a G•U pair shown in cyan. (**B**) The second pair with a shorter inter-metal distance involves a Mg^{2+} of the *mer*-$3O_{ph}.3O_w$ type and a heptacoordinated K^{+} (for density representations, see **Figure S8**). The green and cyan dotted lines correspond to distances below 2.3 Å and in the 2.6–3.2 Å range, respectively. The orange dotted lines mark the inter-metal distance. For clarity, experimental densities and some water molecules are not shown. Mg^{2+} and K^{+} are green and purple, respectively.

References:

1. Bowman, J.C., Lenz, T.K., Hud, N.V. and Williams, L.D. (2012) Cations in charge: magnesium ions in RNA folding and catalysis. *Curr. Opin. Struct. Biol.*, **22**, 262-72.

2. Nierhaus, K.H. (2014) Mg^{2+}, K^{+}, and the ribosome. *J. Bacteriol.*, **196**, 3817-9.

3. Gevrekci, A.O. (2017) The roles of polyamines in microorganisms. *World J. Microbiol. Biotechnol.*, **33**, 204.

4. Trachman, R.J. and Draper, D.E. (2017) Divalent ion competition reveals reorganization of an RNA ion atmosphere upon folding. *Nucleic Acids Res.*, **45**, 4733-42.

5. Bowman, J.C., A.S., P. and Williams, L.D. (2018) Role of cations in RNA folding and function. In Kolb, V. M. (ed.), *Handbook of Astrobiology*. CRC Press, Boca Raton, pp. 421-35.

6. Akanuma, G. (2021) Diverse relationships between metal ions and the ribosome. *Biosci. Biotechnol. Biochem.*, **85**, 1582-93.

7. Belinite, M., Khusainov, I., Soufari, H., Marzi, S., Romby, P., Yusupov, M. and Hashem, Y. (2021) Stabilization of ribosomal RNA of the small subunit by spermidine in *Staphylococcus aureus*. *Front. Mol. Biosci.*, **8**, 738752.

8. Ban, N., Nissen, P., Hansen, J., Moore, P.B. and Steitz, T.A. (2000) The complete atomic structure of the large ribosomal subunit at 2.4 Å resolution. *Science*, **289**, 905-20.

9. Klein, D.J., Moore, P.B. and Steitz, T.A. (2004) The contribution of metal ions to the structural stability of the large ribosomal subunit. *RNA*, **10**, 1366-79.

10. Fromm, S.A., O'Connor, K.M., Purdy, M., Bhatt, P.R., Loughran, G., Atkins, J.F., Jomaa, A. and Mattei, S. (2023) The translating bacterial ribosome at 1.55 A resolution generated by cryo-EM imaging services. *Nat. Commun.*, **14**, 1095.

11. Polikanov, Y.S., Melnikov, S.V., Soll, D. and Steitz, T.A. (2015) Structural insights into the role of rRNA modifications in protein synthesis and ribosome assembly. *Nat. Struct. Mol. Biol.*, **22**, 342-4.

12. Jenner, L.B., Demeshkina, N., Yusupova, G. and Yusupov, M. (2010) Structural aspects of messenger RNA reading frame maintenance by the ribosome. *Nat. Struct. Mol. Biol.*, **17**, 555-60.

13. Gabdulkhakov, A., Nikonov, S. and Garber, M. (2013) Revisiting the *Haloarcula marismortui* 50S ribosomal subunit model. *Acta Crystallogr. D Struct. Biol.*, **69**, 997-1004.

14. Leonarski, F., D'Ascenzo, L. and Auffinger, P. (2019) Nucleobase carbonyl groups are poor Mg^{2+} inner-sphere binders but excellent monovalent ion binders - A critical PDB survey. *RNA*, **25**, 173-92.

15. Leonarski, F., D'Ascenzo, L. and Auffinger, P. (2017) Mg^{2+} ions: do they bind to nucleobase nitrogens? *Nucleic Acids Res.*, **45**, 987-1004.

16. Auffinger, P., Ennifar, E. and D'Ascenzo, L. (2021) Deflating the RNA Mg^{2+} bubble. Stereochemistry to the rescue! *RNA*, **27**, 242-52.

17. Dauter, Z., Wlodawer, A., Minor, W., Jaskolski, M. and Rupp, B. (2014) Avoidable errors in deposited macromolecular structures: an impediment to efficient data mining. *IUCrJ*, **1**, 179-93.

18. Williams, L.D. (2005) Between objectivity and whim: nucleic acid structural biology. *Top. Curr. Chem.*, **253**, 77-88.

19. Minor, W., Dauter, Z., Helliwell, J.R., Jaskolski, M. and Wlodawer, A. (2016) Safeguarding structural data repositories against bad apples. *Structure*, **24**, 216-20.

20. Rupp, B. (2016) Only seeing is believing – the power of evidence and reason. *Postępy Biochemii.*, **62**, 250-6.

21. Rupp, B., Wlodawer, A., Minor, W., Helliwell, J.R. and Jaskolski, M. (2016) Correcting the record of structural publications requires joint effort of the community and journal editors. *FEBS J.*, **283**, 4452-7.

22. Wlodawer, A., Dauter, Z., Porebski, P.J., Minor, W., Stanfield, R., Jaskolski, M., Pozharski, E., Weichenberger, C.X. and Rupp, B. (2018) Detect, correct, retract: How to manage incorrect structural models. *FEBS J.*, **285**, 444-66.

23. Gao, Y., Thorn, V. and Thorn, A. (2023) Errors in structural biology are not the exception. *Acta Crystallogr. D Struct. Biol.*, **79**, 206-11.

24. Zheng, H., Chordia, M.D., Cooper, D.R., Chruszcz, M., Muller, P., Sheldrick, G.M. and Minor, W. (2014) Validation of metal-binding sites in macromolecular structures with the CheckMyMetal web server. *Nat. Protoc.*, **9**, 156-70.

25. Zheng, H., Cooper, D.R., Porebski, P.J., Shabalin, I.G., Handing, K.B. and Minor, W. (2017) CheckMyMetal: a macromolecular metal-binding validation tool. *Acta Crystallogr. D Struct. Biol.*, **73**, 223-33.

26. Gucwa, M., Lenkiewicz, J., Zheng, H., Cymborowski, M., Cooper, D.R., Murzyn, K. and Minor, W. (2023) CMM-An enhanced platform for interactive validation of metal binding sites. *Protein Sci.*, **32**, e4525.

27. Zheng, H., Shabalin, I.G., Handing, K.B., Bujnicki, J.M. and Minor, W. (2015) Magnesium-binding architectures in RNA crystal structures: validation, binding preferences, classification and motif detection. *Nucleic Acids Res.*, **43**, 3789-801.

28. Marcia, M., Manigrasso, J. and De Vivo, M. (2021) Finding the Ion in the RNA-Stack: Can computational models accurately predict key functional elements in large macromolecular complexes? *J. Chem. Inf. Model.*, **61**, 2511-5.

29. Zhou, Y. and Chen, S.J. (2022) Graph deep learning locates magnesium ions in RNA. *QRB Discov.*, **3**.

30. Durr, S.L., Levy, A. and Rothlisberger, U. (2023) Metal3D: a general deep learning framework for accurate metal ion location prediction in proteins. *Nat. Commun.*, **14**, 2713.

31. Zheng, H., Zhang, H., Zhong, J., Gucwa, M., Zhang, Y., Ma, H., Deng, L., Mao, L., Minor, W. and Wang, N. (2024) PinMyMetal: A hybrid learning system to accurately model metal binding sites in macromolecules. *Res Sq*.

32. Wang, K., Yin, Z., Sang, C., Xia, W., Wang, Y., Sun, T. and Xu, X. (2024) Geometric deep learning for the prediction of magnesium-binding sites in RNA structures. *Int. J. Biol. Macromol.*, **262**, 130150.

33. Auffinger, P. (2006) Molecular dynamics simulations of RNA systems: importance of the initial conditions. In Sponer, J. and Lankas, F. (eds.), *Computational studies of DNA and RNA.* Springer Verlag, Vol. II, pp. 283-300.

34. Vaiana, A.C., Westhof, E. and Auffinger, P. (2006) A molecular dynamics simulation study of an aminoglycoside/A-site RNA complex: conformational and hydration patterns. *Biochimie*, **88**, 1061-73.

35. Jung, J., Nishima, W., Daniels, M., Bascom, G., Kobayashi, C., Adedoyin, A., Wall, M., Lappala, A., Phillips, D., Fischer, W. *et al.* (2019) Scaling molecular dynamics beyond 100,000 processor cores for large-scale biophysical simulations. *J. Comput. Chem.*, **40**, 1919-30.

36. Sanbonmatsu, K.Y. (2019) Large-scale simulations of nucleoprotein complexes: ribosomes, nucleosomes, chromatin, chromosomes and CRISPR. *Curr. Opin. Struct. Biol.*, **55**, 104-13.

37. Watson, Z.L., Knudson, I.J., Ward, F.R., Miller, S.J., Cate, J.H.D., Schepartz, A. and Abramyan, A.M. (2023) Atomistic simulations of the *Escherichia coli* ribosome provide selection criteria for translationally active substrates. *Nat. Chem.*, **15**, 913-21.

38. Paternoga, H., Crowe-McAuliffe, C., Bock, L.V., Koller, T.O., Morici, M., Beckert, B., Myasnikov, A.G., Grubmuller, H., Novacek, J. and Wilson, D.N. (2023) Structural conservation of antibiotic interaction with ribosomes. *Nat. Struct. Mol. Biol.*, **30**, 1380-92.

39. Byju, S., Hassan, A. and Whitford, P.C. (2023) The energy landscape of the ribosome. *Biopolymers*, e23570.

40. Auffinger, P., Bielecki, L. and Westhof, E. (2004) Symmetric K^+ and Mg^{2+} ion-binding sites in the 5S rRNA loop E inferred from molecular dynamics simulations. *J. Mol. Biol.*, **335**, 555-71.

41. Auffinger, P., Bielecki, L. and Westhof, E. (2003) The Mg^{2+} binding sites of the 5S rRNA loop E motif as investigated by molecular dynamics simulations. *Chem. Biol.*, **10**, 551-61.

42. Auffinger, P. and Westhof, E. (2001) Water and ion binding around $r(UpA)_{12}$ and $d(TpA)_{12}$ oligomers - Comparison with RNA and DNA $(CpG)_{12}$ duplexes. *J. Mol. Biol.*, **305**, 1057-72.

43. Auffinger, P. and Westhof, E. (2000) Water and ion binding around RNA and DNA (C,G)-oligomers. *J. Mol. Biol.*, **300**, 1113-31.

44. Kirmizialtin, S., Pabit, S.A., Meisburger, S.P., Pollack, L. and Elber, R. (2012) RNA and its ionic cloud: solution scattering experiments and atomically detailed simulations. *Biophys. J.*, **102**, 819-28.

45. He, W., Chen, Y.L., Pollack, L. and Kirmizialtin, S. (2021) The structural plasticity of nucleic acid duplexes revealed by WAXS and MD. *Sci. Adv.*, **7**.

46. Kolev, S.K., St Petkov, P., Milenov, T.I. and Vayssilov, G.N. (2022) Sodium and magnesium ion location at the backbone and at the nucleobase of RNA: Ab Initio molecular dynamics in water solution. *ACS Omega*, **7**, 23234-44.

47. Fujita, K., Shindo, Y., Katsuta, Y., Goto, M., Hotta, K. and Oka, K. (2023) Intracellular Mg^{2+} protects mitochondria from oxidative stress in human keratinocytes. *Commun. Biol.*, **6**, 868.

48. Hsiao, C. and Williams, L.D. (2009) A recurrent magnesium-binding motif provides a framework for the ribosomal peptidyl transferase center. *Nucleic Acids Res.*, **37**, 3134-42.

49. Bowman, J.C., Petrov, A.S., Frenkel-Pinter, M., Penev, P.I. and Williams, L.D. (2020) Root of the tree: The significance, evolution, and origins of the ribosome. *Chem. Rev.*, **120**, 4848-78.

50. Rozov, A., Khusainov, I., El Omari, K., Duman, R., Mykhaylyk, V., Yusupov, M., Westhof, E., Wagner, A. and Yusupova, G. (2019) Importance of potassium ions for ribosome structure and function revealed by long-wavelength X-ray diffraction. *Nat. Commun.*, **10**, 2519.

51. Groom, C.R. and Allen, F.H. (2014) The Cambridge Structural Database in retrospect and prospect. *Angew. Chem. Int. Ed. Engl.*, **53**, 662-71.

52. Taylor, R. and Wood, P.A. (2019) A million crystal structures: The whole is greater than the sum of its parts. *Chem. Rev.*, **119**, 9427-77.

53. Leonarski, F., D'Ascenzo, L. and Auffinger, P. (2016) Binding of metal ions to purine N7 atoms and implications for nucleic acids: A CSD survey. *Inorg. Chim. Acta*, **452**, 82-9.

54. Shields, G.P., Raithby, P.R., Allen, F.H. and Motherwell, W.D. (2000) The assignment and validation of metal oxidation states in the Cambridge Structural Database. *Acta Cryst.*, **B56**, 455-65.

55. Li, Z., Song, L.F., Sharma, G., Koca Findik, B. and Merz, K.M., Jr. (2023) Accurate metal-imidazole interactions. *J. Chem. Theory Comput.*, **19**, 619-25.

56. Afonine, P.V., Poon, B.K., Read, R.J., Sobolev, O.V., Terwilliger, T.C., Urzhumtsev, A. and Adams, P.D. (2018) Real-space refinement in PHENIX for cryo-EM and crystallography. *Acta Crystallogr. D Struct. Biol.*, **74**, 531-44.

57. Emsley, P., Lohkamp, B., Scott, W.G. and Cowtan, K. (2010) Features and development of Coot. *Acta Crystallogr. D Struct. Biol.*, **66**, 486-501.

58. Auffinger, P., Bielecki, L. and Westhof, E. (2004) Anion binding to nucleic acids. *Structure*, **12**, 379-88.

59. D'Ascenzo, L. and Auffinger, P. (2016) Anions in nucleic acid crystallography. *Methods Mol. Biol.*, **1320**, 337-51.

60. D'Ascenzo, L. and Auffinger, P. (2015) A comprehensive classification and nomenclature of carboxyl-carboxyl(ate) supramolecular motifs and related catemers: implications for biomolecular systems. *Acta Cryst.*, **B71**, 164-75.

61. Glusker, J.P., Katz, A.K. and Bock, C.W. (2001) Two-metal binding motifs in protein crystal structures. *Struct. Chem.*, **12**, 323-41.

62. Puyo-Fourtine, J., Juille, M., Henin, J., Clavaguera, C. and Duboué-Dijon, E. (2022) Consistent picture of phosphate-divalent cation binding from models with implicit and explicit electronic polarization. *J. Phys. Chem. B*, **126**, 4022-34.

63. Wang, J., Natchiar, S.K., Moore, P.B. and Klaholz, B.P. (2021) Identification of Mg(2+) ions next to nucleotides in cryo-EM maps using electrostatic potential maps. *Acta Crystallogr. D Struct. Biol.*, **77**, 534-9.

64. Hsiao, C., Tannenbaum, E., VanDeusen, H., Hershkovitz, E., Perng, G., Tannenbaum, A.R. and Williams, L.D. (2009) Complexes of nucleic acids with group I and II cations. In Hud, N. V. (ed.), *Nucleic Acid-Metal Ion Interactions*. Royal Society of Chemistry, Cambridge, pp. 1-38.

65. Petrov, A.S., Bowman, J.C., Harvey, S.C. and Williams, L.D. (2011) Bidentate RNA-magnesium clamps: on the origin of the special role of magnesium in RNA folding. *RNA*, **17**, 291-7.

66. Westhof, E., Watson, Z.L., Zirbel, C.L. and Cate, J.H.D. (2023) Anionic G*U pairs in bacterial ribosomal rRNAs. *RNA*, **29**, 1069-76.

67. Fasnacht, M., Gallo, S., Sharma, P., Himmelstoss, M., Limbach, P.A., Willi, J. and Polacek, N. (2022) Dynamic 23S rRNA modification ho5C2501 benefits Escherichia coli under oxidative stress. *Nucleic Acids Res.*, **50**, 473-89.

68. Ennifar, E., Walter, P. and Dumas, P. (2003) A crystallographic study of the binding of 13 metal ions to two related RNA duplexes. *Nucleic Acids Res.*, **31**, 2671-82.

69. Ihara, T., Ishii, T., Araki, N., Wilson, A.W. and Jyo, A. (2009) Silver ion unusually stabilizes the structure of a parallel-motif DNA triplex. *J. Am. Chem. Soc.*, **131**, 3826-7.

70. Tanaka, Y., Kondo, J., Sychrovsky, V., Sebera, J., Dairaku, T., Saneyoshi, H., Urata, H., Torigoe, H. and Ono, A. (2015) Structures, physicochemical properties, and applications of T-Hg(II)-T, C-Ag(I)-C, and other metallo-base-pairs. *Chem. Commun.*, **51**, 17343-60.

71. Auffinger, P. and Ennifar, E. (2017) Nucleic acid nanomaterials: Silver-wired DNA. *Nat. Chem.*, **9**, 932-4.

72. Grime, G.W., Zeldin, O.B., Snell, M.E., Lowe, E.D., Hunt, J.F., Montelione, G.T., Tong, L., Snell, E.H. and Garman, E.F. (2020) High-throughput PIXE as an essential quantitative assay for accurate metalloprotein structural analysis: development and application. *J. Am. Chem. Soc.*, **142**, 185-97.

73. Holvec, S., Barchet, C., Lechner, A., Fréchin, L., De Silva, S., Hazemann, I., Wolff, P., von Loeffelholz, O. and Klaholz, B. (2023) Structure of the human 80S ribosome at 1.9 Å resolution – the molecular role of chemical modifications and ions in RNA. *BioRxiv*.

74. Yang, W., Lee, J.Y. and Nowotny, M. (2006) Making and breaking nucleic acids: two-Mg2+-ion catalysis and substrate specificity. *Mol Cell*, **22**, 5-13.

75. Palermo, G., Cavalli, A., Klein, M.L., Alfonso-Prieto, M., Dal Peraro, M. and De Vivo, M. (2015) Catalytic metal ions and enzymatic processing of DNA and RNA. *Acc. Chem. Res.*, **48**, 220-8.

76. Correll, C.C., Freeborn, B., Moore, P.B. and Steitz, T.A. (1997) Metals, motifs and recognition in the crystal structure of a 5S rRNA domain. *Cell*, **91**, 705-12.

77. Petrov, A.S., Bernier, C.R., Hsiao, C., Okafor, C.D., Tannenbaum, E., Stern, J., Gaucher, E., Schneider, D., Hud, N.V., Harvey, S.C. and Williams, L.D. (2012) RNA-magnesium-protein interactions in large ribosomal subunit. *J. Phys. Chem. B*, **116**, 8113-20.

78. Cate, J.H., Hanna, R.L. and Doudna, J.A. (1997) A magnesium ion core at the heart of a ribozyme domain. *Nat. Struct. Biol.*, **4**, 553-8.

79. Toor, N., Keating, K.S., Taylor, S.D. and Pyle, A.M. (2008) Crystal structure of a self-spliced group II intron. *Science*, **320**, 77-82.

80. Steinke, F. and Stock, N. (2021) Systematic investigation of new alkaline earth phosphonates based on the linker molecule N,N’‐4,4’‐bipiperidine‐bis(methylenephosphonic acid). *Z. anorg allg. Chem.*, **647**, 1046-51.

81. Green, S.P., Jones, C. and Stasch, A. (2007) Stable magnesium(I) compounds with Mg-Mg bonds. *Science*, **318**, 1754-7.

82. Perera, L., Beard, W.A., Pedersen, L.G. and Wilson, S.H. (2017) Hiding in plain sight: The bimetallic magnesium covalent bond in enzyme active sites. *Inorg. Chem.*, **56**, 313-20.

83. Zhao, H., Lin, Z., Lynn, A.Y., Varnado, B., Beutler, J.A., Murelli, R.P., Le Grice, S.F. and Tang, L. (2015) Two distinct modes of metal ion binding in the nuclease active site of a viral DNA-packaging terminase: insight into the two-metal-ion catalytic mechanism. *Nucleic Acids Res.*, **43**, 11003-16.

84. Yu, T., Jiang, J., Yu, Q., Li, X. and Zeng, F. (2023) Structural insights into the distortion of the ribosomal small subunit at different magnesium concentrations. *Biomolecules*, **13**.

85. Noller, H. (1984) Structure of ribosomal RNA. *Annu. Rev. Biochem.*, **53**, 119-62.

86. Gulen, B., Petrov, A.S., Okafor, C.D., Wood, D.V., O'Neill, E.B., Hud, N.V. and Williams, L.D. (2016) Ribosomal small subunit domains radiate from a central core. *Sci. Rep.*, **6**.

87. Biedermannova, L., Cerny, J., Maly, M., Nekardova, M. and Schneider, B. (2022) Knowledge-based prediction of DNA hydration using hydrated dinucleotides as building blocks. *Acta Crystallogr. D Struct. Biol.*, **78**, 1032-45.

88. Cerny, J., Schneider, B. and Biedermannova, L. (2017) WatAA: Atlas of protein hydration. Exploring synergies between data mining and ab initio calculations. *Phys. Chem. Chem. Phys.*, **19**, 17094-102.

89. Biedermannova, L. and Schneider, B. (2016) Hydration of proteins and nucleic acids: Advances in experiment and theory. A review. *Biochim. Biophys. Acta*, **1860**, 1821-35.

90. Biedermannova, L. and Schneider, B. (2015) Structure of the ordered hydration of amino acids in proteins: analysis of crystal structures. *Acta Crystallogr. D Biol. Crystallogr.*, **71**, 2192-202.

91. Steitz, T.A. and Steitz, J.A. (1993) A general two-metal-ion mechanism for catalytic RNA. *Proc. Natl. Acad. Sci. USA*, **90**, 6498-502.

92. Jacobsen, D.M., Bao, Z.Q., O'Brien, P., Brooks, C.L. and Young, M.A. (2012) Price to be paid for two-metal catalysis: Magnesium ions that accelerate chemistry unavoidably limit product release from a protein kinase. *J. Am. Chem. Soc.*, **134**, 15357-70.

93. Hwang, W., Yoo, J., Lee, Y., Park, S., Hoang, P.L., Cho, H., Yu, J., Hoa Vo, T.M., Shin, M., Jin, M.S. *et al.* (2018) Dynamic coordination of two-metal-ions orchestrates q-exonuclease catalysis. *Nat. Commun.*, **9**, 4404.

94. Trachman, R.J., 3rd and Ferre-D'Amare, A.R. (2021) An uncommon [$K^+(Mg^{2+})_2$] metal ion triad imparts stability and selectivity to the Guanidine-I *RNA*, **27**, 1257-64.

95. Luo, B., Zhang, C., Ling, X., Mukherjee, S., Jia, G., Xie, J., Jia, X., Liu, L., Baulin, E.F., Luo, Y. *et al.* (2023) Cryo-EM reveals dynamics of *Tetrahymena* group I intron self-splicing. *Nat. Catal.*, **6**, 298-309.

96. Spyrakis, F., Ahmed, M.H., Bayden, A.S., Cozzini, P., Mozzarelli, A. and Kellogg, G.E. (2017) The roles of water in the protein matrix: A largely untapped resource for drug discovery. *J. Med. Chem.*, **60**, 6781-827.

97. Wei, W., Luo, J., Waldispuhl, J. and Moitessier, N. (2019) Predicting Positions of Bridging Water Molecules in Nucleic Acid-Ligand Complexes. *J. Chem. Inf. Model.*, **59**, 2941-51.

98. Qin, B., Lauer, S.M., Balke, A., Vieira-Vieira, C.H., Burger, J., Mielke, T., Selbach, M., Scheerer, P., Spahn, C.M.T. and Nikolay, R. (2023) Cryo-EM captures early ribosome assembly in action. *Nat. Commun.*, **14**, 898.

99. Sheng, K., Li, N., Rabuck-Gibbons, J.N., Dong, X., Lyumkis, D. and Williamson, J.R. (2023) Assembly landscape for the bacterial large ribosomal subunit. *Nat. Commun.*, **14**, 5220.

100. Miao, Z., Adamiak, R.W., Antczak, M., Boniecki, M.J., Bujnicki, J., Chen, S.J., Cheng, C.Y., Cheng, Y., Chou, F.C., Das, R. *et al.* (2020) RNA-Puzzles Round IV: 3D structure predictions of four ribozymes and two aptamers. *RNA*, **26**, 982-95.

101. Li, B., Cao, Y., Westhof, E. and Miao, Z. (2020) Advances in RNA 3D structure modeling using experimental data. *Front. Genet.*, **11**, 574485.

102. Yamagami, R., Sieg, J.P. and Bevilacqua, P.C. (2021) Functional roles of chelated magnesium ions in RNA folding and function. *Biochemistry*, **60**, 2374-86.

103. Guth-Metzler, R., Mohamed, A.M., Cowan, E.T., Henning, A., Ito, C., Frenkel-Pinter, M., Wartell, R.M., Glass, J.B. and Williams, L.D. (2023) Goldilocks and RNA: where Mg^{2+} concentration is just right. *Nucleic Acids Res.*, **51**, 3529-39.

104. Yamagami, R., Bingaman, J.L., Frankel, E.A. and Bevilacqua, P.C. (2018) Cellular conditions of weakly chelated magnesium ions strongly promote RNA stability and catalysis. *Nat. Commun.*, **9**, 2149.

105. Yamagami, R., Huang, R. and Bevilacqua, P.C. (2019) Cellular concentrations of nucleotide diphosphate-chelated magnesium ions accelerate catalysis by RNA and DNA enzymes. *Biochemistry*, **58**, 3971-9.

106. Zhang, J.J., Ieong, K.W., Johansson, M. and Ehrenberg, M. (2015) Accuracy of initial codon selection by aminoacyl-tRNAs on the mRNA-programmed bacterial ribosome. *Proc. Natl. Acad. Sci. USA*, **112**, 9602-7.

107. Pape, T., Wintermeyer, W. and Rodnina, M. (1999) Induced fit in initial selection and proofreading of aminoacyl-tRNA on the ribosome. *EMBO J.*, **18**, 3800-7.

108. Liebschner, D., Afonine, P.V., Moriarty, N.W., Poon, B.K., Chen, V.B. and Adams, P.D. (2021) CERES: a cryo-EM re-refinement system for continuous improvement of deposited models. *Acta Crystallogr. D Struct. Biol.*, **77**, 48-61.

109. Moore, P.B. (2021) The PDB and the ribosome. *J. Biol. Chem.*, **296**, 100561.

110. Vicens, Q. and Kieft, J.S. (2022) Thoughts on how to think (and talk) about RNA structure. *Proc. Natl. Acad. Sci. USA*, **119**, e2112677119.

111. Hennings, E., Schmidt, H. and Voigt, W. (2013) Crystal structures of hydrates of simple inorganic salts. I. Water-rich magnesium halide hydrates $MgCl_2.8H_2O$, $MgCl_2.12H_2O$, $MgBr_2.6H_2O$, $MgBr_2.9H_2O$, $MgI_2.8H_2O$ and $MgI_2.9H_2O$. *Acta Cryst.*, **C69**, 1292-300.

112. Gerasimchuk, N.N. and Dalley, N.K. (2004) Demetallation of a Ni(II) tetraazamacrocyclic complex by cyanoxime resulting in the formation of a stereospecific trinuclear compound $[Na(H_2O)_6]^+[NaNi_2L_6]^-$ (L = NC-C(NO)-C(O)NH_2^-). *J. Coord. Chem.*, **57**, 1431-45.

113. Noeske, J., Wasserman, M.R., Terry, D.S., Altman, R.B., Blanchard, S.C. and Cate, J.H. (2015) High-resolution structure of the *Escherichia coli* ribosome. *Nat. Struct. Mol. Biol.*, **22**, 336-41.